DIVERTOR TOKAMAK ASDEX

The ASDEX Group

IPP III/27 July 1976

MAX-PLANCK-INSTITUT FÜR PLASMAPHYSIK

8046 GARCHING BEI MÜNCHEN

MAX-PLANCK-INSTITUT FÜR PLASMAPHYSIK

GARCHING BEI MÜNCHEN

DIVERTOR TOKAMAK ASDEX

The ASDEX Group

IPP III/27 July 1976

Die nachstehende Arbeit wurde im Rahmen des Vertrages zwischen dem Max-Planck-Institut für Plasmaphysik und der Europäischen Atomgemeinschaft über die Zusammenarbeit auf dem Gebiete der Plasmaphysik durchgeführt.

IPP III/27

Divertor Tokamak ASDEX

The ASDEX Group

July 1976

Preface

This report compiles 8 papers presented by the ASDEX group at two conferences in November 1975 and June 1976, respectively and is intended to give a summary of the technical concept and status of the ASDEX tokamak.

The first two papers, entitled

The Design of the ASDEX Tokamak, and

The Toroidal and Poloidal Magnetic Field Coils of the ASDEX Tokamak

give a general view of the technical concept of ASDEX. They have been presented at the 6th Symposium on Engineering Problems of Fusion Research, San Diego, USA, November 18 - 21,1975.

The following six papers which have been presented at the 9th Symposium on Fusion Technology, Garmisch-Partenkirchen, Germany, June 14 - 18,1976 describe more detailed topics of the ASDEX project:

Design and Manufacture of the ASDEX Toroidal Field Coils

Technical Concept for the Multipole Coils of ASDEX

The ASDEX Ohmic Heating Electrical System

The Power Supply for the Poloidal Field Coils of ASDEX

Investigation on the Feedback System of ASDEX

Divertor Pumping System of ASDEX

THE DESIGN OF THE ASDEX TOKAMAK

R.Allgeyer, E.Broser, H.Frey, G.Haas, G.Herppich, O.Jandl, M.Keilhacker, M.Kornherr, N.Niedermeyer, W.Poschenrieder, H.Preis, H.Rapp, F.Schneider, G.Siller, F.Wagner, H.Wedler, F.Wesner.

Abstract

ASDEX is a large tokamak (major radius 1.64 m, plasma radius 0.4 m) with axisymmetric (poloidal) divertor now under construction at IPP Garching and scheduled for commissioning in summer 1978. The toroidal field of 3.0 T (on the plasma axis) is produced by 16 D-shaped, water cooled coils. To induce the plasma current of 500 kA (q = 3) the primary current of an air core transformer is interrupted by a D.C. breaker. The vertical field is feedback controlled. The multipole (divertor) coils for producing the separatrix are situated inside the vacuum vessel. The vacuum vessel is a welded stainless-steel structure comprising two half-tori which are connected by polyimid insulating gaps. The divertor pump system uses heated volume getters or Ti sublimation on liquid N_2 cooled getter surfaces.

1. Introduction

ASDEX (Axially Symmetric Divertor EXperiment) is a tokamak with magnetic limiter and axisymmetric (poloidal) divertor /1/ now under construction at IPP, Garching. The experiment is expected to be completed and operational in summer 1978.

The principal objective of the experiment is to test and improve the effectiveness of divertors in reducing the influx of impurities from the walls in high-performance tokamaks. Further points of interest are the MHD stability of tokamak discharges without material limiter for various

shapes of plasma cross-section (D-shape, small vertical elongation) and the effect of the changed boundary conditions on plasma stability (flat current profile) and transport processes (trapped ion mode regime).

Figs.1 and 2, which show a full-scale model of ASDEX (one quarter section), give an overall view of the experiment. Fig. 3 shows a cross-sectional view of ASDEX.

The main parameters of ASDEX are:

Major radius R	1.64 m
Minor radius a	0.40 m
Toroidal field $B_t(R)$	3.0 T
Plasma current $I_p(q = 3)$	500 kA
Flat-top time t_{FT}	5 s
Ion temperature$^+$ T_i	2 keV
Electron temperature$^+$ T_e	4 keV
Plasma density n	$2 \times 10^{13} cm^{-3}$
Confinement time$^+$ ($\tau_p \approx \tau_E$)	0.2 s

$^+$Estimated from transport code (10x pseudoclassical or 6-regime model)

The toroidal field is produced by 16 D-shaped coils. The vacuum vessel consists of two half-tori with insulating gaps in between. The vessel contains the axisymmetric multipole coils which produce the separatrix. The two divertor chambers on top and bottom are separated from the discharge chamber by metal partitions which have toroidal slit apertures to accommodate the scrape-off layer.The entire assembly can be parted on a major diameter and the two halves rolled apart for installation purposes.

While this paper deals with the overall design of ASDEX the toroidal and poloidal magnetic field coils are described in more detail in an accompanying paper /2/.

2. Toroidal Field Coils

The coil system comprises 16 identical D-shaped coils which are supported on a central column along the straight section. The copper winding forms a compact unit. It is elastically mounted along the curved outer side in a stainless-steel casing completely surrounding it, and is only in contact with the casing at the two plane side faces and at the straight support surface. This concept allows free expansion of the winding when heated and complete transmission of the centripetal force to the central column and of the tilting forces (Lorentz forces to the main field coil as a result of poloidal magnetic fields) to the structure, which laterally supports the coils at two points on top and two at the bottom.

The intrinsic forces of the coil system are taken up by the copper windings, whose shape was optimized in such a way that the bending stress is below the permissible limit. It was found that optimization has to be pushed very far. It also became clear that the copper windings are basically subjected to shear stress at the ends of the rigid support surface, and that this cannot be counteracted completely by optimizing the coil shape. In our case the maximum shear stress is 40 kg/cm^2, which means a safety margin of three. The average tensile stress in the copper is 460 kg/cm^2. Due to bending it reaches 710 kg/cm^2 in the inner winding at the point where the radius of curvature is smallest.

During a discharge the coils are heated by a maximum of 40^{o} C and cool down again during the intervals. For this purpose the copper conductor has a circular cooling bore along the center through which water circulates. Numerical calculations showed that direct admission of cold water into the hot coils

causes very large temperature gradients and unacceptable mechanical stress. The water therefore circulates continuously in the coils and is slowly cooled in the intervals by introducing cold water. Each coil is divided into six separate cooling circuits.

3. Support Structure

The support structure (Figs.1 and 3) serves for holding the toroidal field coils, takes up the magnetic forces acting on the toroidal field coils (centripetal and tilting forces) and transfers the weight of the experiment to the foundation. It comprises a central support column, a top and a bottom cover plate, an outer jacket and a carriage for a half-section of the framework.

The central support column, which has to take up the centripetal forces (1.14×10^6 kg per coil) and a certain torsional moment, is a sixteen-cornered column which consists of cemented wooden plates (laminated wood strengthened with epoxy) in order to avoid eddy currents (due to current variations in the OH transformer). Intermediate layers fitted between the column and the toroidal field coils are intended to ensure the closest possible fit of the toroidal field coils to the central support column since slight bending of the straight section of the coil already causes appreciable shear stress in the copper pack.

The top and bottom cover plates each consist of a disc-like inner part made of austenitic cast iron divided into eight insulated segments in order to prevent current loops and 16 box-sectioned supports of the same material which connect the disc with the outer jacket of the structure.

Ready access to the experiment is ensured by making the diameter of the outer jacket of the structure so large that an

approx. 2 m wide gangway is left between the main field coils and the outer jacket (Fig.3). The outer jacket was designed as a zig-zag frame structure in which the eight junctions of the top cover plate are connected with those of the bottom plate, which are displaced 22.5°, by means of push-pull rods.

4. Vacuum Vessel

The vacuum vessel (Figs.2 and 3) is a welded stainless-steel structure. It consists of two half-tori which are connected by insulating gaps made of polyimid. The cross-section of the vessel was fitted to the shape of the toroidal field coils by slanting the top and bottom areas. The vessel contains ten manholes with a width of 600 mm and numerous smaller openings for pumping, neutral injection, diagnostics and for installation purposes.

The divertor chambers on top and bottom are separated from the plasma region by metal partitions which have toroidal slit apertures, 5 cm wide, to accommodate the scrape-off layer. Spars for fixing the multipole coils divide each divertor chamber into 16 sections. The divertor components (collector plates, pumps) are located in removeable inserts with cooled outer walls in order to allow thermal and mechanical separation from the vacuum vessel.

The vessel is to be baked to 150° C (desorption of adsorbed water) by means of overheated water. For this purpose a system of pipes is soldered to the outer walls of the vessel and covered with thermal insulation. The same system of pipes is also being used for cooling the vessel after baking.

Provisions are being made for incorporating a replaceable thin-walled liner which can be heated up to 400° C with induced alternating currents. The liner consists of individual

stripes whose thickness varies in the poloidal direction in order to achieve a constant power density.

5. Divertor Pumps and Vacuum System

In order to accomplish a gas backstreaming ratio R_{H_2}, a pumping speed of

$$S = L\left(\frac{1 - \sigma_H}{R_{H_2}} - 1\right)$$

in the divertor is mandatory (L = conductance of the divertor slit, σ_H = trapping efficiency of the collector rails for plasma ions). At a slit width of 5 cm and a length of the divertor throat of 10 cm we have $L = 6 \times 10^5$ l/s. A backstreaming ratio $R_{H_2} = 0.1$ is planned.

For the pumping system in the divertor two different concepts are being pursued in parallel.

a) Volume getters: Here we investigate the use of ST 101 (Zr-Al) coated getters. The intrinsic pumping speed of this material is 2 l/scm^2, and by arranging the coated strips in concertina fashion (SORB-AC^{TM} cartridge /3/) it is possible to install a total pumping speed of up to 2×10^6 l/s for H_2 in the divertor sections. For a backstreaming ratio of $R_{H_2} = 0.1$ the pumping action will still have to be supported by trapping of energetic plasma protons in the collector rails. Measurements on Zr have shown that trapping efficiencies of $\sigma_H > 0.5$ can be obtained for proton energies > 300 eV /4/, which would be in accord with our requirements. H_2 forms a pseudo-hydride with Zr and can be expelled by heating the collector rails to above 500° C.

The working temperature of the ST 101 getters and the collector rails is 200 to 300° C. The activation tempera-

ture - to remove superficial O_2, N_2 and CO by bulk diffusion - is 700° C. The capacity of the collector rails between regeneration should be sufficient for several 100 shots, whilst the ST 101 cartridge pumps should last for at least 10^5 shots (2×10^6 mbarl H_2). The non-reversible capacity for the active gases O_2, N_2 and CO is about 4×10^5 mbarl.

b) Ti sublimation pumps: A backstreaming ratio of $R_{H_2} = 0.1$ can be achieved even without pumping action of the collector rails ($\sigma_H = 0$). The necessary pumping speed is $S = 6 \times 10^6$ l/s. Assuming an intrinsic pumping speed of 10 l/scm^2 for H_2 at LN_2 temperature, a getter area of 6×10^5 cm^2 is required. For ASDEX this means that the surface area of the cryo getter panels has to be slightly increased as compared to the area of the divertor walls. In each of the 32 divertor chambers we plan to use 2 Ti-sublimator units each comprising 14 Ti-Mo filaments. For each shot up to 0.4 gr of Ti is evaporated. The filaments have to be replaced after approximately 3000 shots.

The design of the getter panels utilizes serrated aluminium plates which provide the required area increase. Tubes are welded to the edges of the plates. This tubulation is part of a closed cooling system through which liquid nitrogen circulates at a pressure of 10 bar. Dangerous local boiling is thereby prevented. Part of the cooling system is also a heat exchanger to keep the temperature at 80 K.

The concept is to be decided at the beginning of 1976. As can already be seen, each represents an entirely feasible alternative. Volume getter pumps, at the present stage, are more expensive but appear more compatible with fusion reactor environments since they work at elevated temperatures and can pump tritium reversibly.

The design of the external vacuum system is influenced by the presence of the powerful internal divertor pumps. In principle, its application could be limited to pump-down after venting and to handling rare gases and such saturated hydrocarbons as are not removed by gettering. However, it should also permit experiments at an early stage without activated divertor pumps. A further point is fast removal of contaminants during discharge cleaning, and also of large amounts of H_2 during regeneration of volume getters.

We have considered the utilization of turbomolecular-pumps as well as cryopumps with and without cryosorption. We finally decided in favour of a system consisting of 8 turbomolecular pumps each with 3500 l/s air speed. Considering all the specific conditions and dimensions of our experiment, we believe this to be the most economical, most flexible, and least troublesome solution. Because of the fairly long tubulation - necessitated not least by the extent of the magnetic field - about one half of the normal speed, i.e. 14000 l/s will be available at the torus. Without the divertor pumps activated, a base pressure in the low 10^{-8} range is expected since the vacuum vessel contains some components not compatible with UHV technology.

6. Ohmic Heating System and Vertical Field Coils

The ohmic heating and vertical field coils (and also the multipole compensation coils; see next section) are situated in between the vacuum vessel and the toroidal field coils (Figs.2 and 3). They are attached to the frame of the toroidal field coils in such a way that they can expand in the radial direction and only vertical forces are transferred to the toroidal coils.

Since the entire experiment can be parted on a major diameter for installation purposes, all poloidal field coils are as-

sembled from half-coils (180^{o} sections) with separable, bolted winding connections.

The 100-turn OH transformer consists of 24 single coils with between 1 and 6 turns. They are distributed around the vacuum vessel in such a way that the stray field in the plasma region is minimum ($<10^{-3}$ T).

To induce the plasma current, the current in the primary is interrupted by a D.C. breaker and commutated in a resistor.

After current zero negative current rise is possible.

The vertical field is produced by single-turn coils and is feedback controlled (see section 9).

7. Multipole (Divertor) Field Coils

The choice of the poloidal magnetic field configuration is governed by the following aims:

- stability of plasma column
- favourable position of divertor
- optimum utilization of magnetic field

For these reasons a "double inside divertor" (stagnation points above and below the plasma, slightly displaced towards the axis) as shown in Fig.2 was chosen. To get short-range divertor fields with minimum distortion of the plasma equilibrium, the separatrix is produced by a multipole triplet with zero net current (quadrupole field). To further improve the concept of a "localized divertor", the multipole triplet is supplemented by additional series-connected coils outside the vacuum vessel which compensate the divertor field over the major part of the plasma region. The shape of the plasma cross-section and the stability of the plasma are then

almost exclusively determined by the vertical field. While the vertical field must be time-dependent, the currents in the multipole coils can now be constant in time, which is, of course, a great technical advantage.

The multipole coils (Figs.2 and 3) have circular cross-sections and are built up of 4 and 8 turns respectively. They are embedded in vacuum-tight jackets each consisting of 16 bellow sections and 16 solid rings. The coils are attached to the spars of the vacuum vessel by these rings via spring elements in such a way that they can expand on being heated and only vertical forces are transferred to the vacuum vessel.

The multipole coils are series-connected with the toroidal field coils. In normal operation (full plasma current) the multipole currents are constant in time, their amplitude being varied by shunts. At reduced plasma current, however, the multipole coils can be operated with time-dependent currents by using one of the two converter modules (see next section).

8. Power Supply System

The toroidal field is supplied by a flywheel generator with a rectifier diode bridge. The maximum power of the generator is 155 MW, its energy 1.45 GJ. The maximum D.C. voltage is 3.3 kV at a D.C. current of 45 kA.

The ohmic heating transformer is fed from a 15 MJ flywheel generator via a mercury static converter. During flat-top, current inversion is possible within the limits of the energy left in the generator (5 to 6 MJ).

The fast rise of the vertical field requires a powerful energy source and a static converter as the regulating unit of a feedback system. Since the large generator for the toroidal field

has no power left and other sources are not at our disposal, the vertical field coils are connected in series with the toroidal field coils. The latter represents a constant current source. The vertical field current will be controlled by a bypass static converter as shown in Fig.4.

The commutation of the converter is done by means of the generator's 3-phase AC voltage, but the power for the vertical field rise comes from the toroidal field. The reaction on the toroidal field can be neglected.

This concept has mainly been chosen because of its high adaptability to changes in the experimental parameters and in the coil circuitry. Its technology is commonly known. Alternative solutions which have been studied are the D.C. current chopper and an independent static converter system with a 3-phase capacitor network. In all cases the vertical field coils are in series with the toroidal field coils.

The vertical field converter consists of two modules in parallel each of them with a current rating of 22.5 kA/5 s and a maximum D.C. output voltage of 1200 V. The pulse number is 12 for both modules in parallel.

With toroidal field currents lower than specified the power capacity of the generator will be sufficient for supplying the vertical field current in the conventional way. In this case the vertical field coils and the toroidal field coils can be disconnected.

The stationary coupling of the vertical field parameters to the toroidal field current is an inherent disadvantage of the chosen concept. As far as the currents are concerned, this can be overcome by changing the mode of operation as

shown in Fig.5. The exciting or de-exciting voltage for the vertical field, however, can be adapted only by changing the transformer windings, if necessary.

When the plasma current is reduced, the multipole current may be controlled separately with one of the two converter modules. This can be accomplished in the same way as above. Depending in the toroidal field current, either the normal operation or the by-pass mode of operation is more favourable.

The circuitry of the axisymmetric coils is flexible. This makes possible the shunting of single coils, the change of polarity and the exchange of power sources. In particular, it opens the possibility of producing non-circular plasma cross-sections by driving a non-zero net current through the multipole coils.

Our considerations concerning the radial field and its amplifier are not yet finished. Our concept of producing an opening magnetic limiter during plasma current build-up by shifting the plasma in the vertical direction imposes rather high requirements on the power consumption of this system.

9. Vertical Field Feedback System

The vertical field is operated with the described thyristor converter. Stabilization of the plasma is achieved with a closed and programmed control circuit (Fig.6).

Copper shells are not provided, but the vacuum vessel has a stabilizing effect, brief though it may be. As theoretical determination of this effect is scarcely possible owing to the complicated shape of the vessel with divertor chambers and separating slit, a 1 : 10 model of ASDEX was built to measure the couplings and characteristic values. The plasma

was thereby simulated with several copper rings which could be electronically switched on, off or over.

The dynamic properties and the performance of a 6-pulse thyristor controller were investigated experimentally (380 V, 10 A) and theoretically.

These test values were used to define the controlled system (including the passive feedback) and to find the optimum controller for the purpose (Fig.6).

The active controlled member I comprises the following elements:

a) Vertical field coil; τ = 150 ms

b) Coupling to vessel k = 0.7

c) Vessel penetration time constant of vertical field τ = 12 ms

d) Effective vessel slit 1.2 m

The passive feedback II involves the following features:

a) Centering mirror currents in the vessel during plasma current formation; τ = 8 ms, center R_p = 1.5 m

b) Mirror currents in the vessel due to radial plasma shift; τ = 1.4 ms

c) Centering induction currents in the vertical field coil during plasma current formation; τ = 150 ms, center R_p = 1.4 m

d) Induced currents in the vertical field coil due to plasma shift; τ = 150 ms

e) Coupling of the plasma current to the OH transformer; k = 0.47, τ = 12 or 560 ms

f) Laws of (poloidal and toroidal) flux conservation

g) Field gradient of the vertical field

h) Various plasma parameters are treated in the control circuit as disturbance variables.

Various types of active controllers III and IV with proportional, differential and integral character were investigated. According to the results obtained hitherto most success seems to be afforded by the arrangement with two loops (cascade control) sketched in Fig.6.

Acknowledgements

The authors wish to acknowledge the contributions of H.Finkelmeyer, F.Gresser, F.Hartz, F.Kerl, G.Klement, G.Mühlbauer, F.Werner and many others in the design of this experiment.

References

/1/ W.Feneberg, Phys.Lett.,A,36 (1971) 307
W.Feneberg, K.Lackner, Nucl.Fusion 13 (1973) 549

/2/ R.Allgeyer et al., The Toroidal and Poloidal Magnetic Field Coils of the ASDEX Tokamak, next paper

/3/ SAES Getters, Milan, Via Gallarate 215, Italy

/4/ J.Bohdansky, J.Roth and W.Poschenrieder, Inst.Phys. Conf.Ser.No.28 (1976) 307

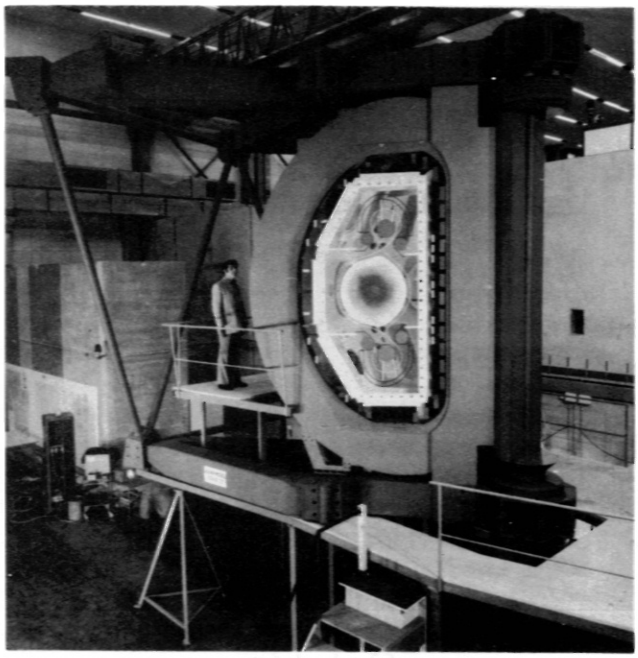

Fig.1:Full-scale model of ASDEX
(one-quarter section)

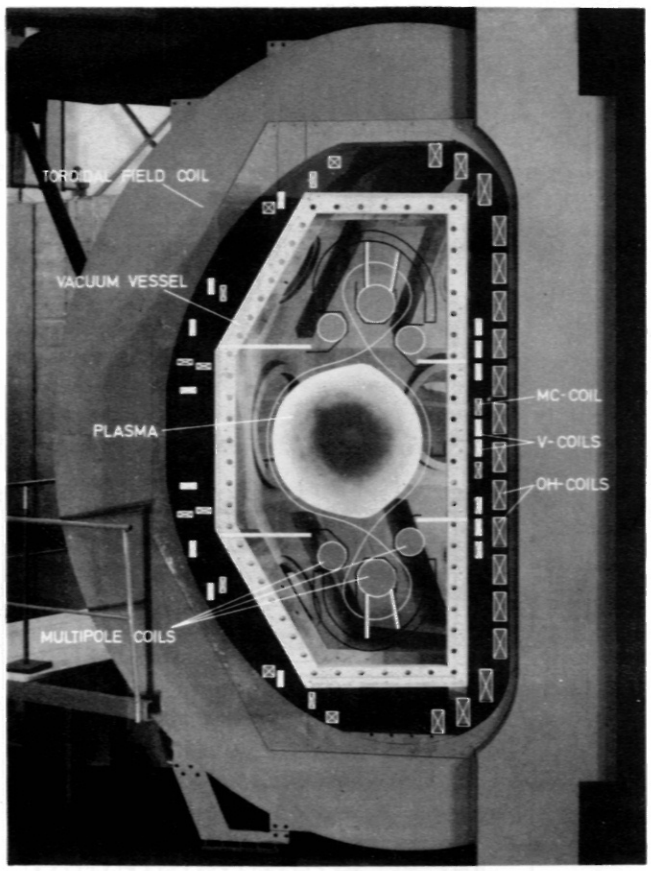

Fig.2: Model of ASDEX showing magnetic field coils and vacuum vessel

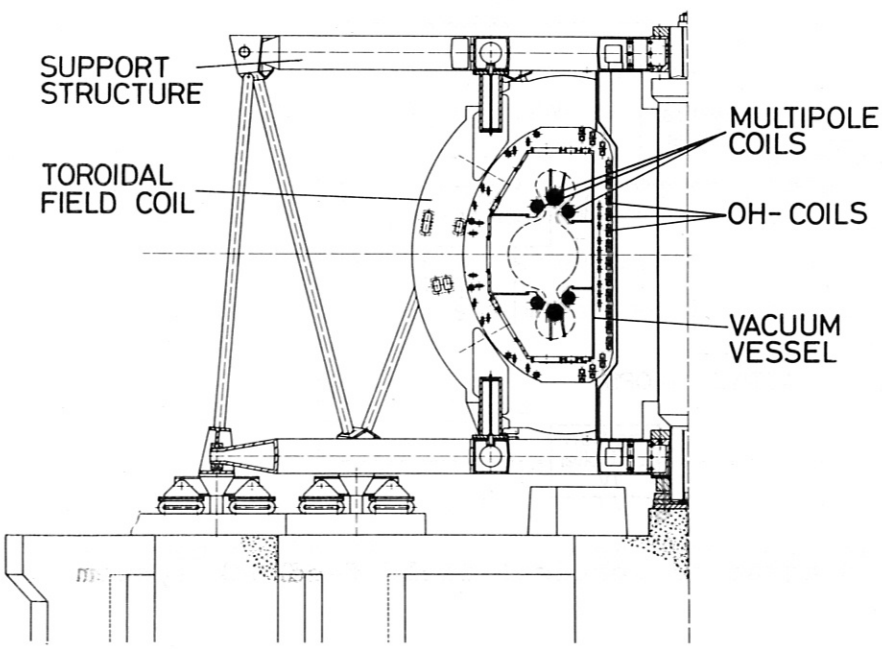

Fig.3: Cross-sectional view of ASDEX

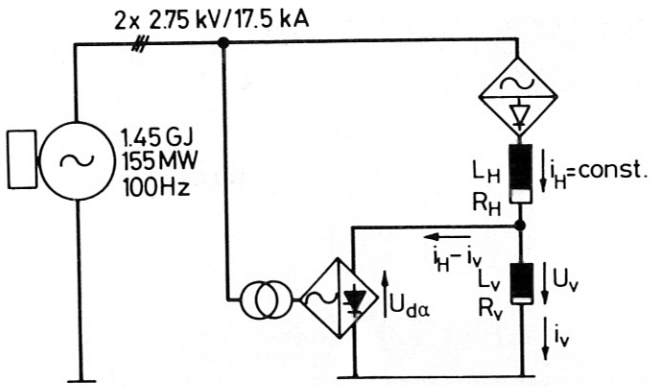

Fig.4: Circuit diagram of toroidal and vertical field power supply

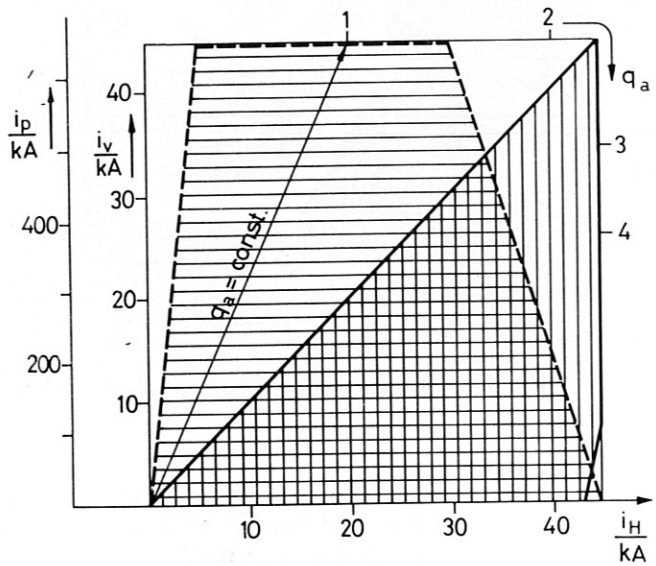

Fig.5: Coupling of toroidal and vertical field parameters during flat-top;
——— limits of by-pass operation mode
---- limits of normal operation mode

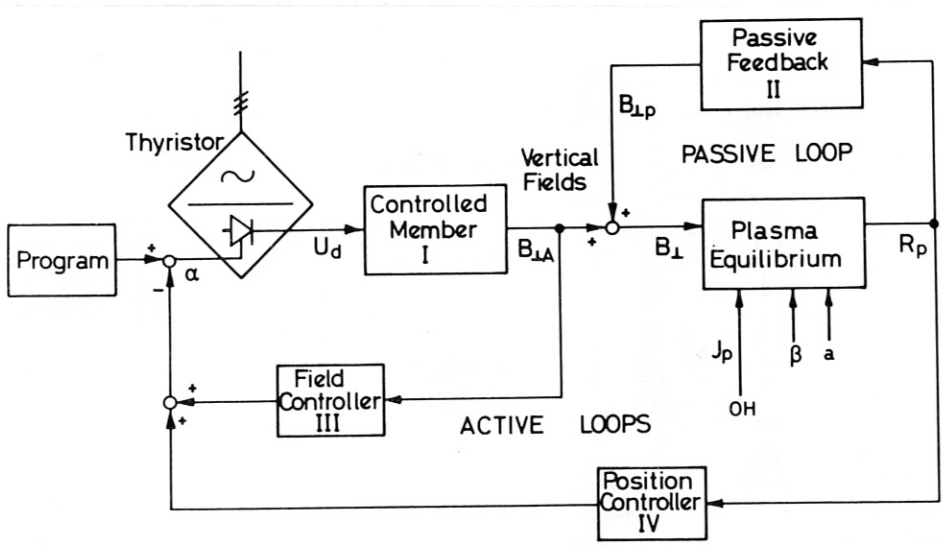

Fig.6: Block circuit diagram of vertical field feedback system

THE TOROIDAL AND POLOIDAL MAGNETIC FIELD COILS OF THE ASDEX TOKAMAK

R.Allgeyer, E.Broser, M.Keilhacker, M.Kornherr, H.Niedermeyer, H.Preis, H.Wedler, F.Wesner.

Abstract

The design of the magnetic field coil system of the ASDEX tokamak is described. It consists of 16 toroidal field coils, producing a magnetic field of 3 T in the plasma center and of 54 poloidal field coils to induce the plasma current, to stabilize the plasma position and to produce an axisymmetric divertor field.

1. Introduction

ASDEX is a divertor tokamak with circular plasma cross-section and two axisymmetric divertors one above and one below the plasma region. Therefore, the vacuum vessel has an elongated cross-section and the toroidal field coils are D-shaped. All poloidal field coils are situated inside the toroidal field coils, and the multipole coils for producing the divertor field are inside the vacuum vessel (Fig.1). The whole experiment can be divided into two halves in order to install the poloidal field coils and the vacuum vessel.
In the following the toroidal and poloidal magnetic field coils of ASDEX are described while the overall design of the experiment is given in an accompanying paper /1/.

2. Toroidal Field Coils

The toroidal magnetic field is produced by only 16 equal, D-shaped coils /2/. The copper windings are fully embedded

in stainless-steel casings by which the magnetic forces are transmitted to the support structure. This concept allows maximum accessibility to the discharge and divertor chambers.

Calculation

The magnetic field of the non-circular coils was calculated numerically applying Biot and Savart's law, each winding being replaced by a finite number of filament loops, and the coil shape being simulated by polygons. The inductances of the coil system were determined by calculating the self and mutual inductances of all filament loops and by adequate addition.

On the basis of the magnetic field calculation, the poloidal field distribtuion and the support conditions, the mechanical stresses were determined by two-dimensional calculations with a finite element program. The finite shape of the coils was found by minimizing the bending and shear stresses.

The resulting centripetal force acting on one coil is about 10^7 N, against which the coils are supported by a central column. By interaction with the poloidal field a torque on each coil of about 1.2×10^6 Nm with respect to its radial axis is produced. Against these twisting forces the coils are supported by a mechanical structure.

Design

Main data of the toroidal field coils:

Magnetic field in the plasma center	3 T
max. coil current	45 kA
flat-top time	5 s
current rise time	5 s
copper cross section	78 x 22.5 mm

ohmic resistance at 20^{o} C	3.27 mΩ/coil
temperature rise	40 K per pulse
max. temperature	80^{o} C
cooling duct diameter	14 mm
height	4.3 m
width	2.8 m
tensile stress in the copper	33 to 70 N/mm^2
shear stress	4 N/mm^2

The coils consist of a copper winding (1 in Fig.2) and a stainless-steel casing (2). Each copper winding comprises two pancakes with 16 turns each and is wound from copper bars about 5 m long which are brazed together. The brazing joints are distributed along the circumference of the winding (straight part and large radius of curvature). In the straight part, the winding is tapered at its outer three turns. There the copper bars have to be machined before being insulated and wound. The pancake connection and the current leads (3) are situated above and below the mid-plane, alternating from coil to coil.

Each coil is divided into 6 cooling circuits connected in parallel. To keep the thermal stress within tolerable limits, the cooling water is permanently circulated in the coils and heated with the copper. In the pulse intervals the coils are cooled down slowly by mixing with cold water. In the cooling period the maximum temperature difference in the coil is about 25 K. The temperature gradient in one cooling circuit is nearly constant.

The winding is elastically embedded in the stainless-steel casing and pressed against its front plate (8) by means of

a pre-stressed rubber layer (7) at the curved outer side. In this way thermal expansion and perfect transmission of the centripetal force to the central column are possible. To allow thermal expansion while the centripetal force is acting, a very low coefficient of friction between the winding and the straight front plate of the casing must be achieved by a sliding layer (9).

To transfer the twisting forces to the support structure, the winding touches the side plates of the casing, which are strengthened in their central straight part by wedge-shaped supports (10).

3. Poloidal Field Coils

The poloidal field coil system consists of the ohmic heating (air-core) transformer-coil (2 in Fig.1) to induce the plasma current, the vertical field coils (3) to stabilize the plasma position and the multipole coils (4) to produce the divertor field, which is largely compensated in the plasma region by compensating coils (5).

Since the whole experiment can be divided into two halves for installation purpose, all poloidal field coils are composed of half turns, which are screwed together with detachable joints.

Ohmic Heating Transformer Coils

The ohmic heating transformer consists of 24 separate coils with 100 turns altogether, which are distributed between toroidal field coils and vacuum vessel in such a way that the stray field in the plasma region does not exceed 10^{-3} T.

Figure 3 shows two typical half-coils with the turn- and coil-crossovers. The half-turns are connected by bridges which are pressed on the turn ends by pre-stressed copper-beryllium bands (Fig.4).

The ends of the half-turns and the bridges have to be machined very exactly. The toothed joints ensure a sufficiently small transition resistance and largely torque-free taking over of the tensile forces.

The radial expansion forces have to be taken up by the copper turns themselves by tensile stress. Against the vertical compression forces the coils are supported by holders attached to the casings of the toroidal field coils.

All inner transformer coils are clamped together and secured against movements in the toroidal direction at 4 points on the circumference.

The 100 turns are divided into 26 parallel cooling circuits. The nearly adiabatically heated coils are cooled down in the pulse intervals by cold water.

To induce a current in the plasma, the current is interrupted by a D.C. breaker and commutated in a resistor.

In order to reduce the pulse voltage in the interruption period, the coils are electrically divided into an upper and lower part and grounded in the midplane.

After current zero a negative current rise is possible to bring about a flat-top plasma current

Main data of the ohmic heating coils:

Max. current	30 kA
Rise time	0.5 s
Interruption time	15..50 ms
Max. coil voltage	20 kV
Max. voltage to earth	10 kV

Max. magnetic flux	3 Vs
Max. magnetic field	1 T
Copper cross-section	930 mm^2
Cooling duct diameter	8 mm
Temperature rise per pulse	14° C
Max. temperature	60° C
Max. tensile stress	20 N/mm^2
Max. axial force	33 tons per coil

Multipole Coils

The two triplets of multipole coils (one 8-turn coil and two 4-turn coils) to produce the separatrix and the divertor field are situated within the vacuum vessel above and below the plasma region (Fig.1).

The coils are composed of copper bars with cross-sections like sectors of a circle. Figure 5 shows how the machine ends of the half-turns are connected by screwed joints, which have to be fitted exactly.+)

The coils are embedded in vacuum-tight stainless-steel jackets, consisting of bellows and 16 rings with which the coils are attached in the vessel.

By these attachments, which allow radial thermal expansion, the coils are supported against vertical components of the magnetic forces which act on the coils. The radial components are taken up by the copper turns themselves.

All coils are connected in series. The current direction is such that no resulting current is induced by the transformer coils.

+) After this paper had been presented in November 1975, the cross sections and the joint-design were changed in order to improve the mechanical strength of the coils. The new coil design is described in the 4th paper of this report.

The 4-turn coils have one, the 8-turn coils two cooling circuits in parallel. To reduce thermal stress the cooling procedure is the same as in the toroidal field coils.

Main data of the multipole coils:

Max. current	45 kA
Max. pulse times as for toroidal field coils	
Copper cross-section	1600 mm^2
Cooling duct diameter	14 mm
Temperature rise per pulse	40 K
Max. temperature (baking out temperature of the vacuum vessel)	150° C
Max. tensile stress in the copper	30 N/mm^2
Max. vertical force component on one coil	78 tons

Multipole-Compensating Coils and Vertical Field Coils

The vertical field and multipole-compensating coils are situated outside the vacuum vessel (Fig.1). Their half-turns are connected in the same way as the ohmic heating half-coils (Fig.4). These coils are directly cooled by cold water. They are attached to the toroidal field coils together with the ohmic heating. As with the multipole coils no resulting current is induced by the transformer coils.

Main data of these coils:

Max. current	45 kA
Max. pulse times as for toroidal field coils	
Copper cross-section	1600 mm^2

Cooling duct diameter	14 mm
Max. temperature rise per pulse	40 K
Max. temperature	80° C

4. Powering of the Coils

The toroidal field coils and the multipoles with their compensating coils are powered in series by a 1.5 GJ fly-wheel generator with silicon diodes. The current in the multipoles can be varied by means of shunts. The vertical field coils are also powered by this generator, but their current is controlled by a thyristor converter as part of a feedback-system. By means of this converter and reduced power, or in a later state of the experiment by means of a new planned generator, it is also possible to work with time-dependent multipole currents.

Acknowledgements

The authors wish to acknowledge the contributions of W.Bitter, F.Hartz, F.Kerl, G.Klement, P.Martin and many others in the design of this experiment.

References

/1/ R.Allgeyer et al., The Design of the ASDEX Tokamak, preceding paper

/2/ E.Broser et al., The Toroidal Magnetic Field Coils for the ASDEX Tokamak, Proc.5th Internat.Conf.on Magnet Technology, Roma 1975, p.332

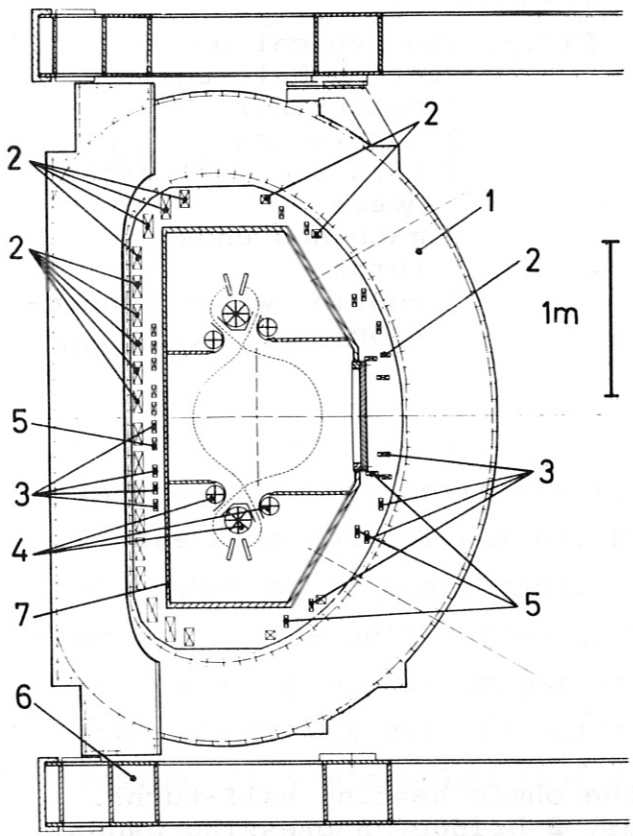

Fig.1: Magnetic field coil configuration
1 toroidal field coil
2 ohmic heating coils
3 vertical field coils
4 multipole coild
5 multipole compensating coils
6 mechanical structure
7 vacuum vessel

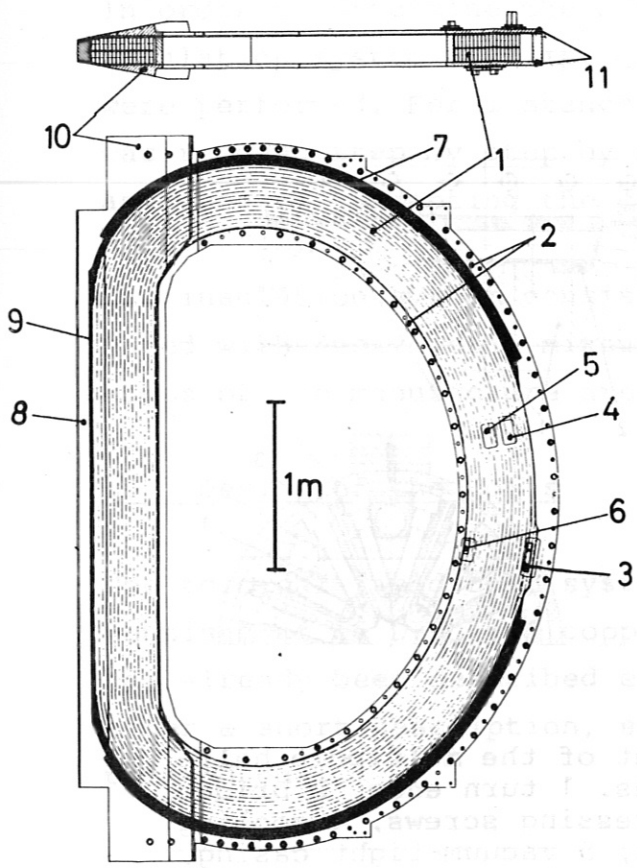

Fig.2: Toroidal field coil design
1 copper winding
2 stainless-steel casing
3 current lead and water inlet
4 water outlets
5 water inlets
6 water outlets at the pancake connection
7 rubber layer
8 front plate of the casing
9 sliding layer
10,11 wedge-shaped support and side plate of the casing

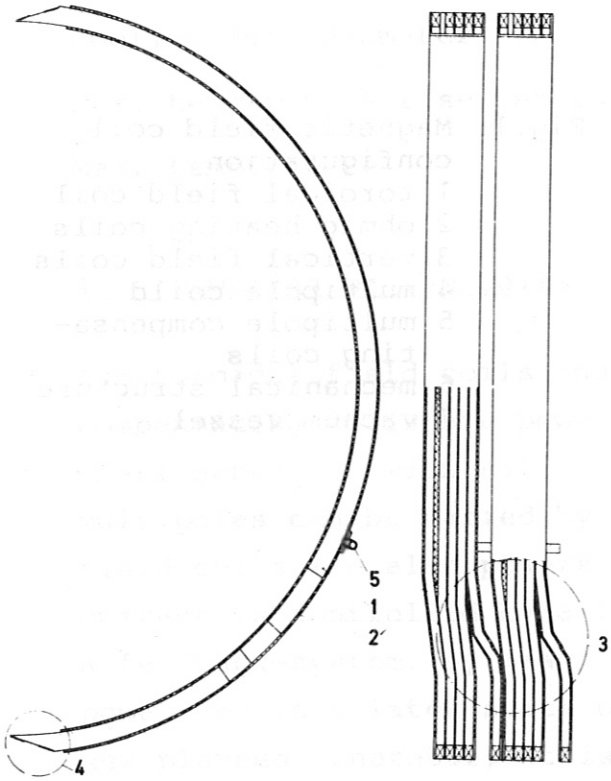

Fig.3: Two typical ohmic heating half-coils
1 copper bar
2 insulation
3 turn and coil cross-overs
4 machined ends of turns
5 cooling water connection

Fig.4: Joint of the ohmic heating half-turns. 1 turn ends, 2 bridge, 3 pressing bands, 4 cooling duct, 5 and 6 turn and joint insulation

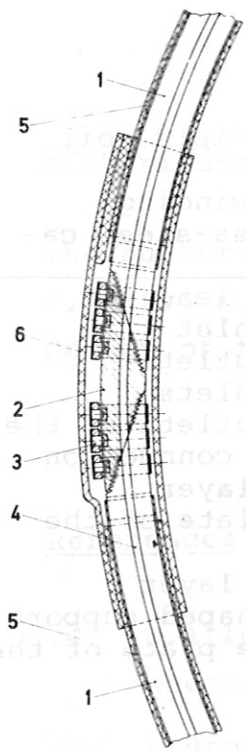

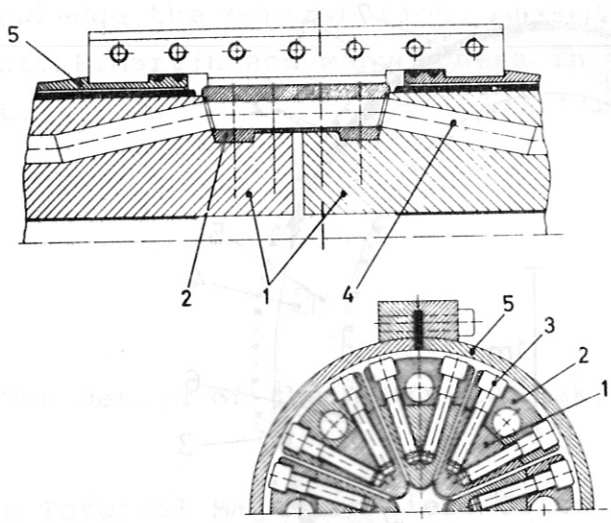

Fig.5: Joint of the multipole half-turns. 1 turn ends, 2 bridge, 3 pressing screws, 4 cooling duct, 5 vacuum-tight casing.

DESIGN AND MANUFACTURE OF THE ASDEX TOROIDAL FIELD COILS

E.Broser, K.-J.Greve[+)], M.Keilhacker, M.Kornherr, R.K.Maix[+)], H.Niedermeyer, H.Preis, J.Rauch[+)], F.Wesner.

Abstract

Each coil consists of a vacuum impregnated winding embedded in a casing. The coils are supported against the centripetal forces by a central column. Forces due to the poloidal field are taken up by the casing. The D-shape minimizes bending caused by the self-forces of the coil system. These forces are taken up by the copper itself. The finite element program STRUDL was used to calculate stresses in winding and casing. It was checked that the design is insensitive to the variations of the elastic properties of the windings.

In order to determine the best suitable winding procedure, insulation system and impregnation method several tests were performed. For instance, the theoretical coil shape was reached step by step by making full scale test windings and gradually adapting the coil former.

The insulation system consists only of glass fabric impregnated with epoxy resin mixture. The most important critical steps of the manufacture are described in this paper.

1. Design of the Coils

The toroidal field coil system of the ASDEX divertor tokamak consists of 16 D-shaped copper coils (Tab.1). Their design has already been described earlier /1/,/2/. In this paper, after a short description, some special details shall be pointed out.

[+)] BBC Brown, Boverie & Cie.,Ltd., Baden (Switzerland) and Mannheim (F.R. of Germany)

Concept of Design

A vacuum impregnated double pancake winding is embedded in a stainless-steel casing (Fig.1). It may freely expand in the winding plane and is supported laterally by the casing. Thus, forces caused by the poloidal fields are taken up by the casing. The self-forces of the coil system are taken up by copper or, in the straight section, by a central column, respectively. The casing consists of an inner and an outer ring, a top plate and a bottom plate. Plates and rings are connected by bolts, the bottom plate is additionally connected with both rings by a series of short and narrow welding seams. The casing can be considered a bent box beam.

The Winding

For ease of manufacturing the cross-section of the winding has been chosen rectangular with the exception of the straight section, which is slightly tapered. The shape has been iteratively optimized with respect to small shear stress using the finite element program STRUDL. Plane stress elements of constant thickness were used, the tapering was neglected. The nodal force was correctly calculated by numerical integration of the volume force multiplied by the shape function of the element. Since the elastic properties of a copper winding are not properly defined, the (anisotropic) elastic constants were varied over an order of magnitude. The tensile stress component parallel to the conductor shown in Fig.3 depends only slightly upon the constants chosen. Plots of the displaced geometry do not show any bending deformation. The tensile force is constant within 1 % along the circumference. It can be concluded that the optimum shape has been approximated very well and that this optimum shape is determined mainly by the equilibrium condition.

The tensile stress is not constant over the cross-section. The contour of the coil is enlarged self-similarly while the radial thickness of the winding is reduced due to con-

tracition. This means higher strain values at the inner edge of the winding than at the outer edge. (The relative increase of the inner circumference is higher than of the outer one). Within the straight supported section this bending moment must nearly vanish. The transition from homogeneous to inhomogeneous stress distribution causes a peak of shear stress at the ends of the straight section. It is requested that the insulation between the turns should withstand a shear stress of 0.5 kg/mm^2 with a high safety margin, and that brazed joints should not break at a stress of less than 15 kg/mm^2.

The finite element model ignores discontinuities as for example the ends of the conductor. These details were treated analytically.

The stress analysis has also been performed for a single coil. It is found that in a single coil at a current of 26 kA the shear stress is as high as in the coil system at 45 kA.

The Casing

Stresses and deformation of the casing were also calculated applying the STRUDL program. Only 2-dimensional elements were used, the properties of which were varied in several runs. Details, for instance bolts, were ignored. The calculations served to find out critical parts of the construction. In this final version the casing will have sufficient stiffness also for loading the coil by the poloidal field of a plasma configuration which perhaps might be planned in the future.

2. Manufacture of the Coils

Each ASDEX toroidal field coil consists of a vacuum impregnated double pancake, embedded in a stainless-steel casing. Therefore the manufacture has to be made in three steps, namely the fabrication of the double pancake and of the steel casing and the assembly of both.

Fabrication of the Double Pancake

The D-shaped double pancake having 2.8 x 4.3 m outer dimensions and weighing 4.6 t is continuously wound around a coil former which is positioned at the centre of a winding lathe with vertical axis.

As the conductor is delivered in unit lengths of approximately 6 m, a large number of brazed joints per pancake has to be made. In order to develop an adequate brazing technique for the rather flat rectangular copper profile (22.5 x 78 mm, with a 14 Ø hole) a series of brazing tests were made. These tests resulted in a brazing jig consisting of a stable clamping and milling device, which ensures the mating surfaces to be parallel. Through the use of a powerful medium frequency heating device short brazing times were achieved.

The temperature during the brazing operation is controlled by a pyrometer. Further conditions for good quality joints are the use of the surfaces and a brazing technique using a silver-phosphor material without flux.

After being brazed the conductor passes through a brake block, giving a draw during winding of 60 N/mm^2 on the conductor. This causes a draw out of the softened region around the brazed joints, resulting in a rehardening of the copper from 42 HB to 55 HB, as compared to the original half hard condition of 80 HB.

After passing through a sand blasting chamber the conductor is insulated with one layer (1/2 overlapped) of this strength glass fabric tape and wound on the coil former. As additional turn to turn insulation two preimpregnated (B-stage) glass fabric tapes are wound in parallel to the conductor.

After the first layer being wound, the interlayer insulation consisting of several sheets of glass fabric is put on and subsequently the second layer of the double pancake is wound

on top of this, after having been brazed to the special cross-over piece on the coil inside.

Due to the use of half hard copper the pancake relieves after opening of the fixing jigs and removal from the coil former. Therefore, a number of 1 : 1 scale test windings and a gradual adaption of the coil former were necessary to achieve a shape close to the theoretical coil shape and within the defined tolerances. For instance, the conductor has to be overbent in the straight part of the coil, as can be seen in Fig.4.

The three outermost layers are partially wound from premilled conductor bars in order to achieve the wedge shape of the straight part of the coil. Thanks to this machining of the coil impregnation is prevented.

Ground Insulation and Impregnation

After being removed from the winding lathe the outer ground insulation is applied. It consists of several layers of glass fabric tape.

Thereafter the double pancake is put into a special impregnation mould and is, after a dry state induced voltage test, vacuum impregnated with the BBC EP-337 epoxy resin mixture at approximately 80° C. After breaking the vacuum and an overpressure phase polymerizing takes place in an oven at approximately 140° C.

This insulation system has been selected after extensive sample testing with regard to shear strength.

The final shape of the so made double pancake corresponds within ± 3 mm with the specified shape.

Fabrication of the Steel Casings

The casing which completely envelopes the pancake is made of a magnetic stainless-steel in DIN 1.4311 quality. A nitro-

gen additive increases the yield point at 270 N/mm^2. The permeability of this material lies under 1.01.

The casing consists essentially of an inner and an outer ring and the two side plates made of plasma cut steel sheets, welded together with the accurately machined wedge shaped front parts. All parts are welded or bolted together.

In a large number of test weldings the welding electrode Sécheron L 190 was found to be the best suitable. Permanent control of the permeability and careful cleaning during welding operation are essential conditions to continuously achieve welds with low permeability and mechanical strength as required.

Assembly and Tests

For assembly the double pancake is put into the steel casing. Sheets of Teflon-coated brass and stainless-steel between the pancake and the front part of the casing serve as sleeve bearing in order to allow the pancake to expand in spite of the high contact stress during excitation. The pancake is elastically supported and pressed against the front part of the casing by a pretensioned rubber layer. A putty layer of filled epoxy resin on the side plates gives a from-fitting contact to the pancakes. To reduce eddy currents between one of the side plates and the outer ring an insulating layer is inserted.

Before and after assembly a number of tests (such as short circuit and high voltage tests) are made in order to guarantee quality standards. 300 thermal cycles were made on the prototype coil at IPP with a coil current of 26 kA during 30 s, corresponding with a temperature rise of approximately 35 °C.

References

/1/ R.Allgeyer et al., Proc.6th Symp.on Engineering Problems of Fusion Research,San Diego 1975, p.378 and p.777

/2/ E.Broser et al., Proc.5th Internat.Conf.on Magnet Technology, Roma 1975, p.332

Table I

ASDEX Toroidal Field Coil System

Number of Coils	16
Turns per Coil	32
Current	Max. 45 kA
Plasma Radius	1.65 m
Magnetic Field (r = 1.65 m)	2.8 T
Magnetic Energy (I = 45 kA)	237 MJ
Dissipated Power (45 kA,40° C)	115 MW
Available Power	150 MW
Available Energy	1.5 GJ
Time Constant of Coil System	4 s
Flat Top Time (I = 45 kA)	Max. 5 s
Repetition Rate (Full Energy)	Max. 20 per h
Copper Profile	78 x 22.5 mm^2
Bore for Cooling	14 mm Ø
Total Weight of Copper	69.000 kg
Height of Casing	4.27 m
Total Weight of one Coil	8.900 kg
Centripetal Force per Coil	$1.1.10^6$ kp
Tensile Stress in Copper	Max. 7.1 kp/mm^2
Shear Stress in Insulation	Max. 0.5 kp/mm^2

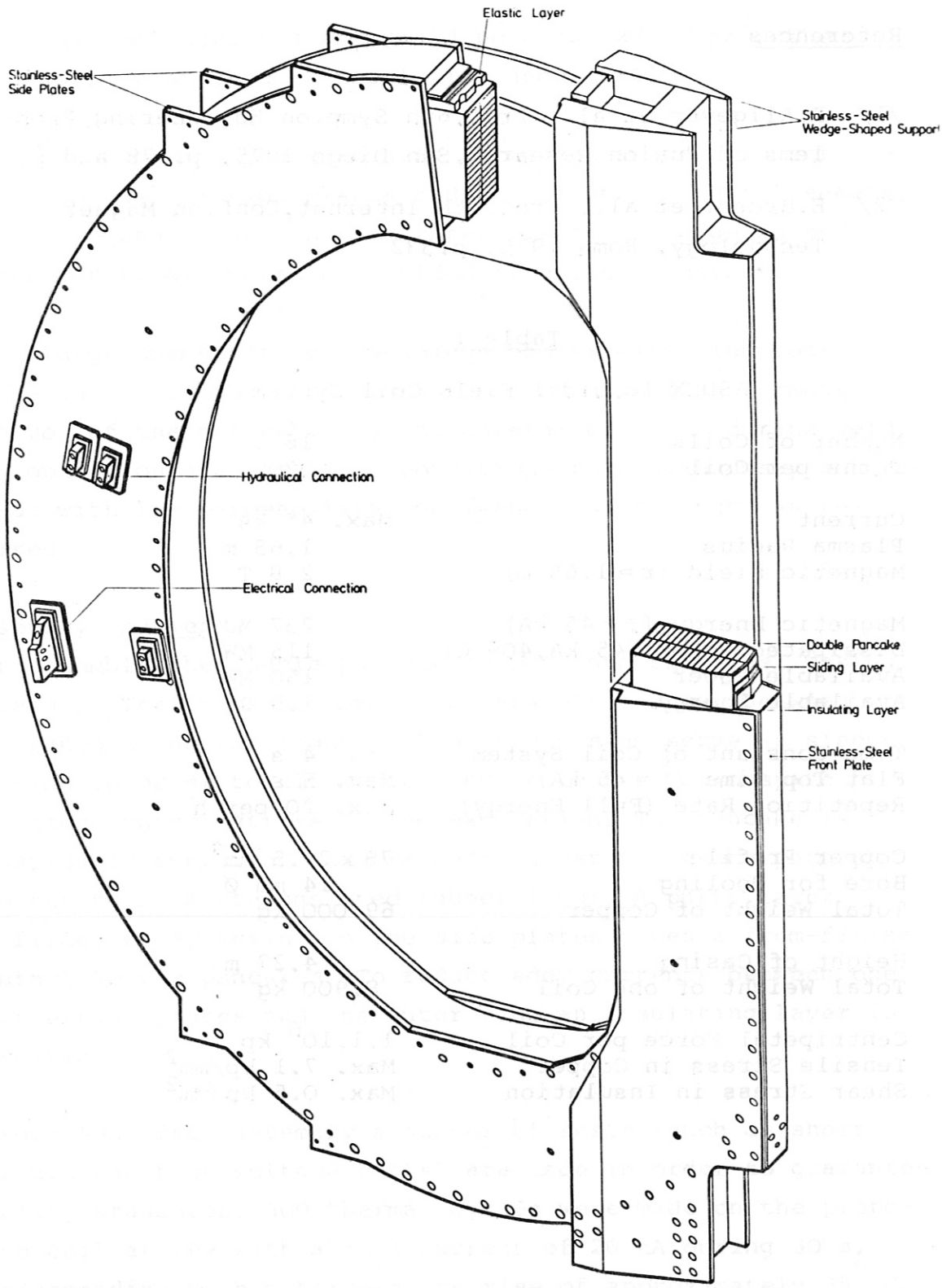

Fig.1: Schematic drawing of the ASDEX toroidal field coil

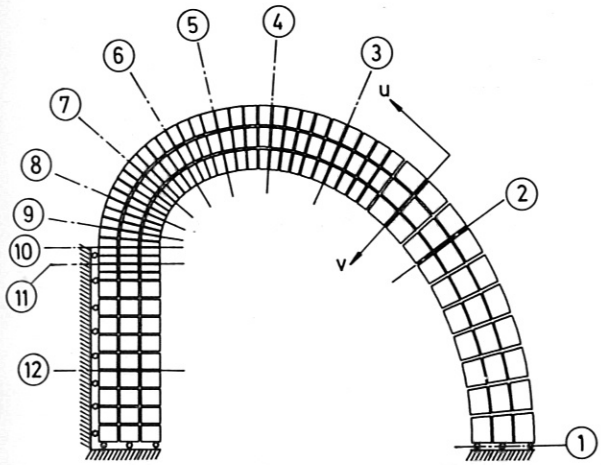

Fig.2: Finite-Element model of ASDEX toroidal field coil

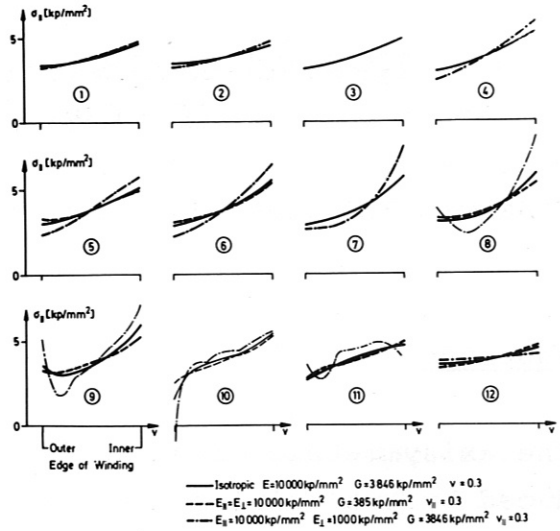

Fig.3: Tensile stress distribu-tribution. Stress component parallel to the axis of the conductor. Loading by the magnetic forces of the coil system

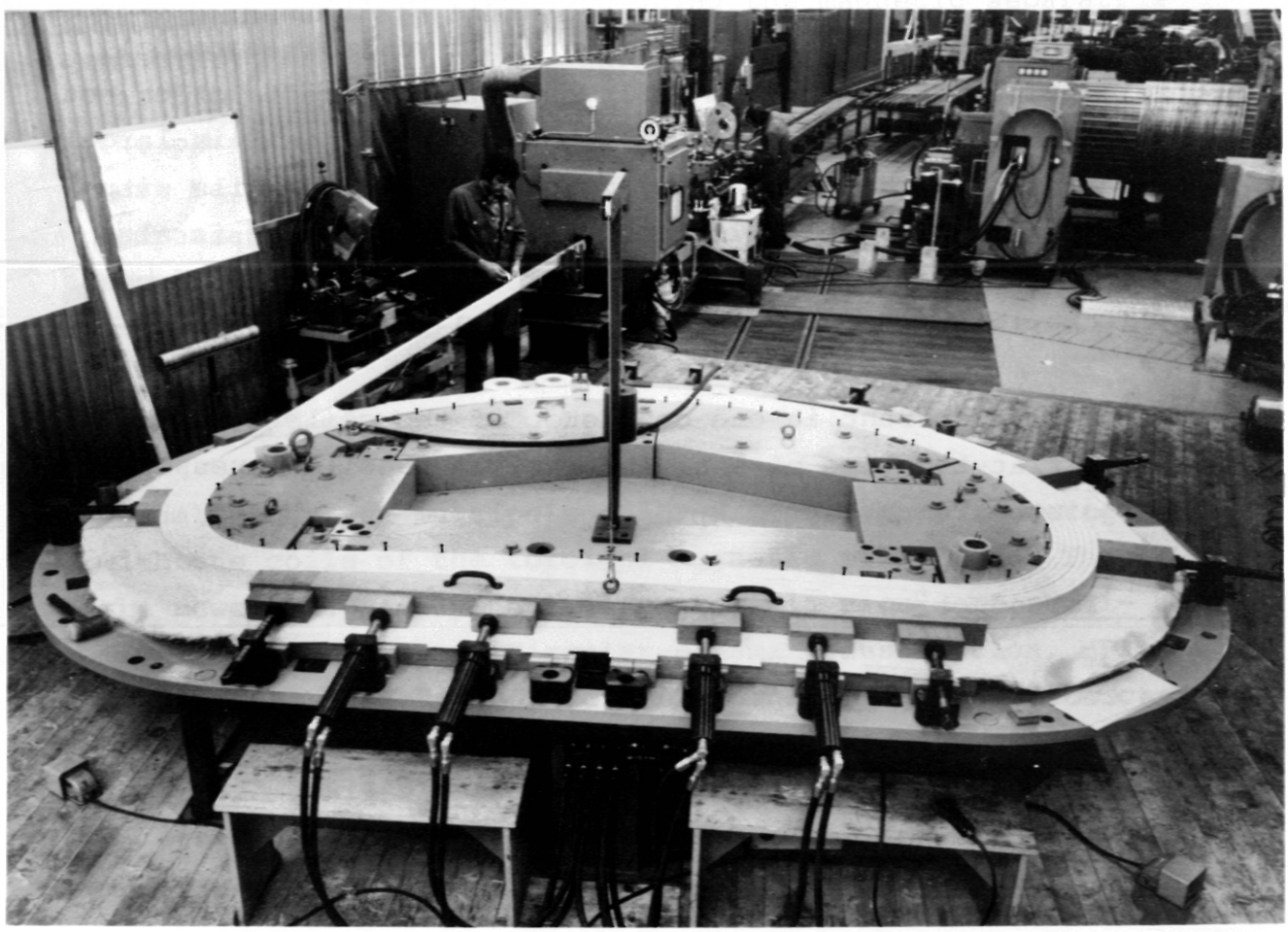

Fig.4: Winding of double pancake

TECHNICAL CONCEPT FOR THE MULTIPOLE COILS OF ASDEX

F.Hartz, P.Krüger, M.Pillsticker, F.Werner, F.Wesner.

Abstract

The axisymmetric divertor field of the ASDEX Tokamak is induced by two triplets of multipole coils situated within the vacuum vessel above and below the plasma region. One coil of a triplet is wound with eight turns and two coils with four turns. The installation of the multipole coils requires, that the coils must be divided into two halves connected by demountable joints. The windings isolated with structural reinforced resin and placed in vacuum-tight stainless-steel bellows are fixed to the vacuum vessel by 16 holdings.

The multipole coils are series-connected with the toroidal field coils and powered by a flywheel generator. In order not to disturb the plasma build up, the multipole field is largely compensated in the plasma region by compensating coils situated outside the vacuum vessel. At reduced power it is also possible to work with time-dependent divertor fields by means of a thyristor converter.

The maximum current in one conductor of the coils is 45 kA with a flat-top time of 5 s. The maximum tensile stresses in the joints are nearly 27 kp/mm^2.

1. Introduction

The two multipole coil triplets of the ASDEX Tokamak induce the magnetic field for the axisymmetric divertor and the magnetic limiter. Therefore, the coils must be fixed near the plasma within the vacuum vessel. These circumstances call for

a special technical concpet for the coils, loaded with a high specific current density and also a high mechanical stress. In addition to this, the installation and the high-voltage loading are problems normally unknown in the production of magnetic coils.

2. Magnetic Field

The two multipole coil(MP) triplets (Fig.1) are symmetrically situated above and below the plasma within the vacuum vessel. The multipole coils MP1 and MP3 are wound in 4 turns and the multipole coils MP2 are wound in 8 turns. Under normal operating conditions the MP1 and MP3 are opposite in series to MP2. The direction of the current in the MP2 and the plasma are equal.

The fundamental effect of the multipole coils for the axisymmetric magnetic field producing the magnetic separatrix is demonstrated in Fig.1 (dotted line). In order to limit the magnetic field effect of the multipole coils within the plasma region, multipole compensation coils (MC coils) must be placed within the axisymmetric coil system. The compensation result shows a comparison of the magnetic potential lines for different energizing conditions of the axisymmetric coils (Fig.2).

3. Layout of the MP Coils

Normally the six multipole coils are connected in series with the coils of the toroidal magnetic main field. They are powered by a flywheel generator via a current rectifier. To induce a non-circular plasma cross-section, MP2 must be fully energized, while MP1 and MP3 are disconnected and only loaded with small equalizing currents. Because the toroidal main field is induced by D-shaped coils that cannot be dismantled, it has to be possible to dismantle all axi-

symmetric coils (MP, MC, ohmic heating OH, vertical V). The MP coils consist of two halves which are force- and current-locked by joints. The current leads-in (Fig.3) to the MP coils are combined by three separate conductors in order to obtain a powerless crossing of high inhomogeneous magnetic fields. The electrical connection of the leads-in of all MP coils takes place for the upper triplet above and for the lower triplet below the vacuum vessel within a region of small magnetic field. For manufacturing reasons the MP coils cannot be helically wound. Each turn is a slotted circular ring connected with the neighbouring ring near the slot. Figure 4 shows a photo of a model of the cross-over region for MP2.
The multipole coils are mounted force-locking to the vacuum vessel by 16 flexible holders.
Regarding the cross-section of the MP coils (Fig.3), the internal conductors are of rectangular cross-section, while the external leads have cross-sections combined by a rectangle and a circular segment in order to take advantage of the available volume for the MP coils.

The fundamental material of the leads is copper (DIN 405000 SE Cu F 30). Because of the high strength in the joints and in the cross-over region we use beryllium copper. All windings are insulated from each other with materials resistant to compression and high voltage. The insulated multipole coils are surrounded with metal bellows which are vacuum-tight and have a high electrical resistance in order to reduce disturbance during the plasma build up. Important dimensions of the coils are given in Tables 1 and 2.

4. Cooling of the Coils

The heat produced by current in the MP leads must be eliminated during current interruption. The cooling medium is unsalted water flowing in a cooling bore inside the leads. For the MP coils there are eight coolant loops working in parallel. Each

MP1 and MP3 is one coolant loop. MP2 is divided into two coolant loops. The water is continuously pumped within the closed loops through a heat exchanger and the leads. We have a flow velocity of nearly 6 $\frac{m}{s}$ and a water pressure of max. 10 $\frac{Kp}{cm^2}$. During the current flow time the cooling water and the leads are heated with $\Delta \vartheta = 51^{o}$ C. The heat dissipation takes place in a controlled manner to reduce thermal stresses. The cooling rate is 0.13 $\frac{dgs.}{s}$ and this gives a temperature drop of 0.18 $\frac{dgs.}{m}$ for the conductor. This means that the temperature drop for a winding is 2 degrees C.

5. Forces and Strengths

The forces stressing the multipole coils are caused by magnetic fields and currents as well as by different thermal elongation.

The thermal elongation of the material produces forces in the radial direction (peripheral forces) resulting in tensile strength. The insulation between the leads is compressed and sheared. These strengths are negligible since they do not determine the dimensions of the multipole coils.

The electromagnetically produced forces result in different strength values within the various regions of a multipole coil.

1) The undisturbed conductor is loaded with line forces in the radial (r) and vertical (z) directions. The r-forces give tensile or compression strength. The z-forces are supported by 16 holders mounted to the vacuum vessel, which results in a bending moment on the conductor. The holder region of a conductor is subject to maximum stress (Fig.6)

2) The joints region is also loaded with r- and z-forces. Because of the reduction of the cross-section in this region higher stresses of the material compared with 1) are obtained.

3) In addition to the r- and z-forces mentioned in 1), the cross-over region is loaded with forces caused by the current cross-over from one conductor to another within the toroidal magnetic field. The external conductors in particular, are very highly stressed.

Table 3 gives a survey of the expected mechanical strength of the single conductors.The total stress on a coil is not the summation of the single conductor stresses because there is a reduction of forces between the conductors. This gives pressure and shearing stresses within the insulation between the layers.

Table 4 shows the resulting forces for the multipole coils under various typical operating conditions.

In order to feed the multipole coils, magnetic fields up to 50 kG have to be crossed with conductors carrying a current of 45 kA. The main forces acting on the multipole feed lines are produced by the toroidal field. They are of the order of 200 kp per cm length of the feed line and are directed radially to the torus. Owing to the opposite polarity of the currents the single conductors either attract or repulse one another, depending on the direction of the toroidal field. Concerning the whole feed line, these forces cancel each other to a large extent if the conductors are frictionally connected. This is attained with the aid of stainless-steel insulated rings mounted around the conductors like pearls on a string. With a simple two-conductor feed line, the remaining forces due to given inhomogenities of the toroidal field would be

of the order of 5 kp/cm or about 0.5 tons, which would necessitate a support structure inside the vacuum vessel. In order to avoid this difficulty, a three-conductor version, shown in Fig.3, was chosen. Owing to this arrangement only forces are generated by fields whose second derivative over r is different from zero. The remaining radial forces are reduced in this way below a level of +/- 0.1 kp/cm and can be neglected.

Forces due to the poloidal fields act in the toroidal direction.

Figure 5 gives the calculated distribution of these forces along the feed lines. The effective forces acting on the three lines are: F1 = -29 kp; F2 = 13 kp; F3 = -12 kp. According to Fig. 7 these forces act mainly in the vicinity of the multipole coils, so that the momentums around the feeding points are kept negligibly small. In order not to insert additional forces due to thermal expansion of the multipole coils, the feed lines are self-supporting. Their connection to the main support structure is made with the aid of flexible conductors.

6. Preliminary Tests

The most critical components of the multipole coils seem to be the joints. They are highly stressed by forces, current, temperature and voltage. Simulated mechanical fatigue tests with joints (Fig. 8) show that no damage occurs with loads 25 % higher than the maximum operating load. Current tests with nominal current on joints with original contacts and tests with current densities twice as high on joints with similar contacts show uncritical temperature rise so that no damage or cold welding could be observed.

Table 1

Dimensions and dates of the multipole coils:

a) mean diameters, MP1: 2709,8 mm
MP2: 3033 mm
MP3: 3454 mm

b) number of turns: MP1: 4
MP2: 8
MP3: 4

c) conductor cross sections
MP1 internal 1446 mm^2
MP3 external 1519 mm^2
MP2 internal 1430 mm^2
external 1432 mm^2

d) cross sestion of cooling bore: 154 mm^2

e) conductor material, 7/8 of turn: SE Cu (DIN Norm)
1/8 of turn: Beryllium Cu

f) electric resistance of the coils,
MP1: 0,46 mΩ
MP2: 1,07 mΩ
MP3: 0,59 mΩ

g) inductivity of the coils
MP1: 0,101 mH
MP2: 0,427 mH total: 0,5628 mH
MP3: 0,138 mH

h) contact surface of the joints: 1730 mm

i) isolation, structural reinforced casting resin;
insulation layer: 2 mm

Table 2

Operating conditions of the multipole coils:

a) current, maximum value: 45000 A
flat top time: 5 s
rise time: 8,5 s
decay time a.
interruption : 5 min.

b) current density, in the conductor: 31,5 A/mm^2
in the joints : 80 A/mm^2
at the contact : 26 A/mm^2

c) contact resistance: 0,6 $\mu\Omega/cm^2$

d) heating/pulse: 51 °C

e) inductive stored energy: 570 kWs

f) heating energy / pulse: 90 MWs

g) voltage drop
inductive, during plasma building up
MP1: 800 V
MP2: 1600 V
MP3: 800 V
ohmic, during flat top time
MP1: 20,7 V
MP2: 48,2 V
MP3: 26,6 V

Table 3

Maximum stresses in multipole conductors

multipole	kind of stress	conductor (fig.5)	k_r (kp/cm) (fig.7)	k_z (kp/cm)	σ_{max} (kp/mm²) conductor	σ_{max} (kp/mm²) joint	σ_{max} (kp/mm²) cross-over
1 or 3	tension	13 14	38 21	-1o -8	6,8 4,4	22 16	19 6,5
1 or 3	tension	4 3	-22 -12	-13 -1o	5 3	16 11	14 4,4
2	tension	9 1o	34 11	-27 33	13 9,5	26 22	27 11,5
2	tension	12 11	-38 -15	25 32	14 9,5	26 22	28 12

Table 4

Forces on multipole coils

operating condition	$K_R = k_R R$ (kp) R radius of coil k_R rad.line load			vertical force (kp)		
	MP1	MP2	Mp3	MP1	MP2	MP3
all axissym coils (nominal) without plasma	814	-5622	8866	-33232	64376	-33402
all axissym.coils (nominal) with plasma	-5289	1852	6667	1177	-1260	11779
all axissym.coils (nominal) noncircular plasma	1130	8484	-826	481	-67362	-1371

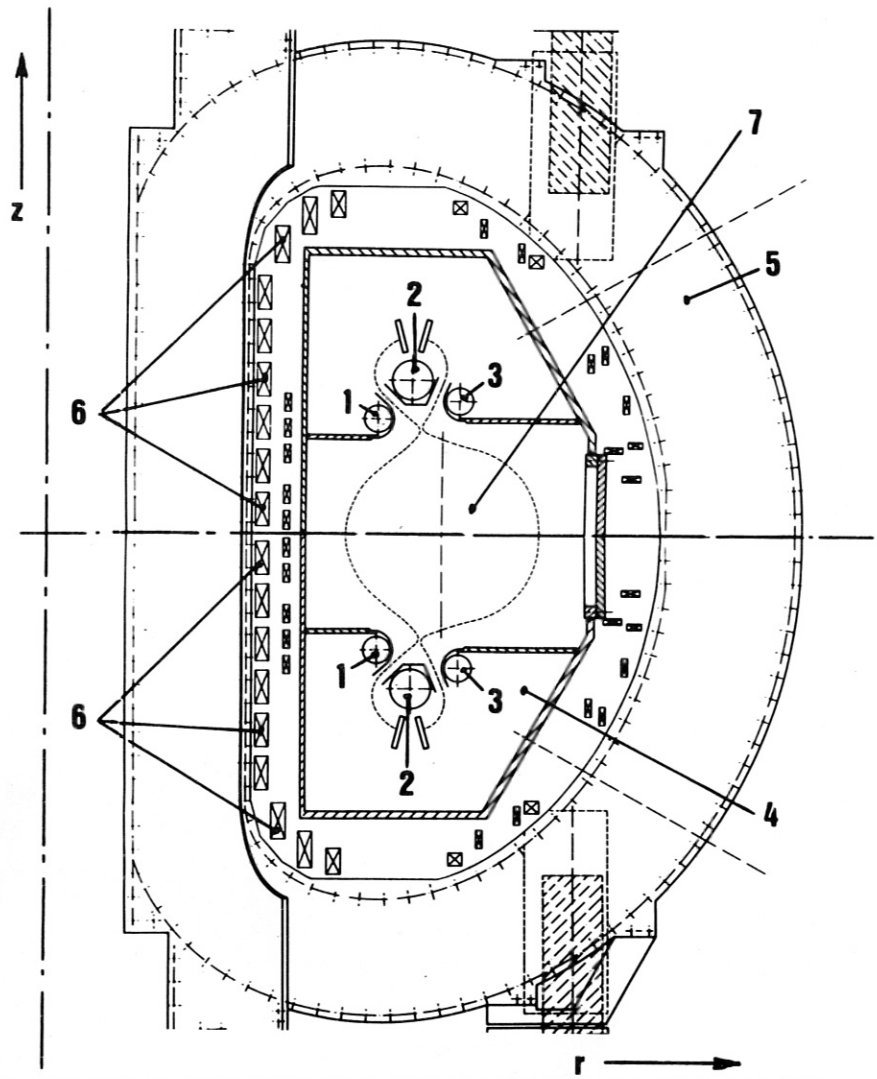

Fig.1: Sectional view of ASDEX
1 Multipole coil MP1
2 Multipole coil MP2
3 Multipole coil MP3
4 vacuum vessel
5 toroidal field coil
6 axisymmetric coils(OH,V,MC)
7 plasma

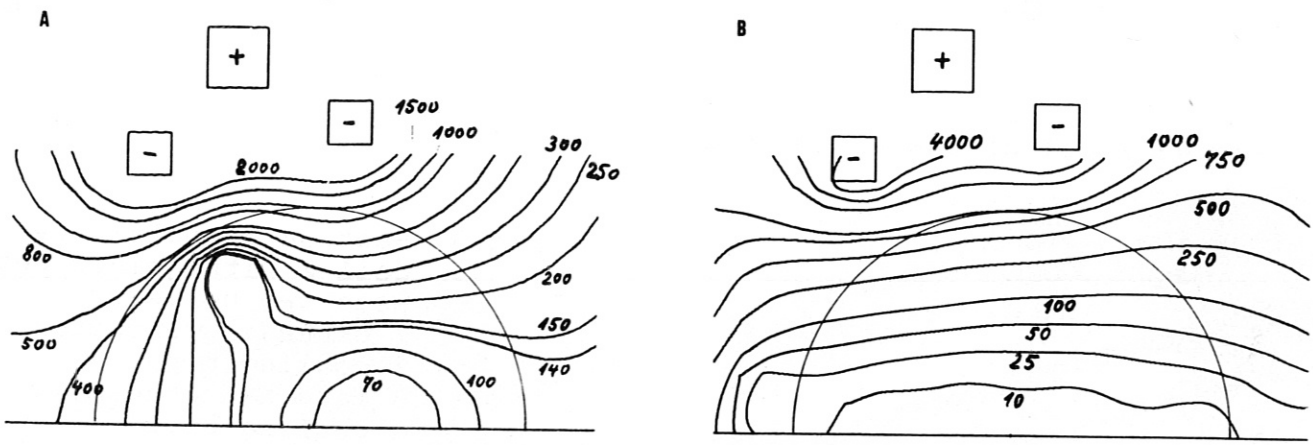

Fig.2: Magnetical potential lines in the plasma region (values in Gaus)

A) of the MP-field

B) of the resulting MP and MC field

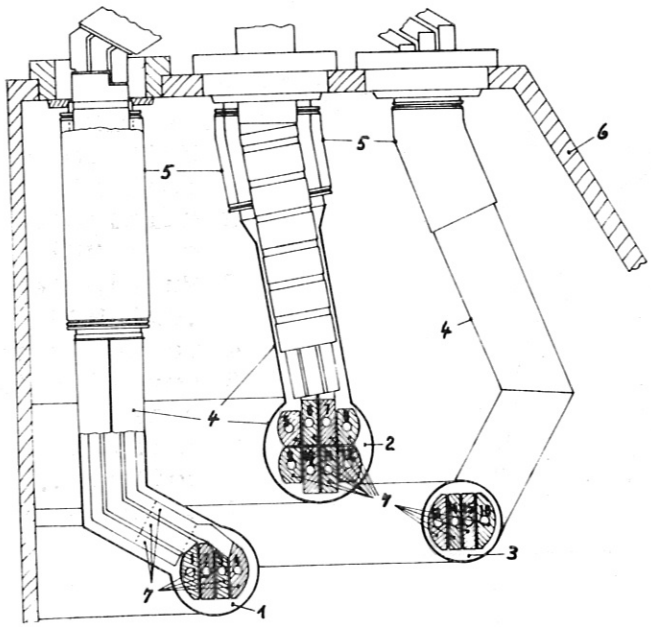

Fig.3: Leads-in for the multipole coils
1 MP1 } with cross-section of the conductors
2 MP2 }
3 MP3 }
4 schield tubes
5 bellows
6 vacuum vessel
7 conductors of the coils and leads-in

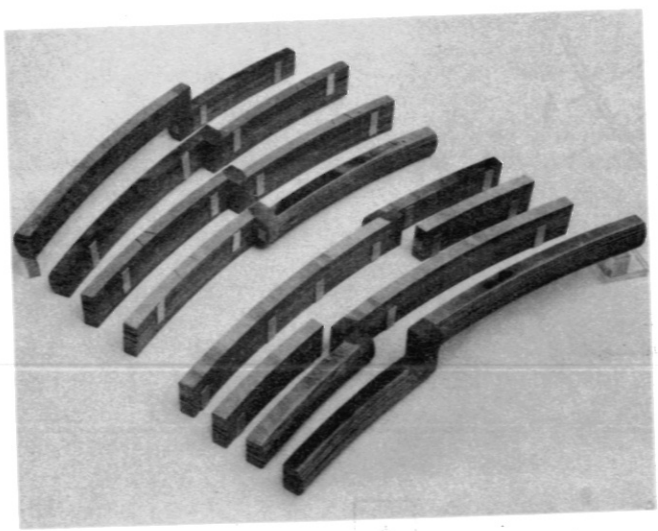

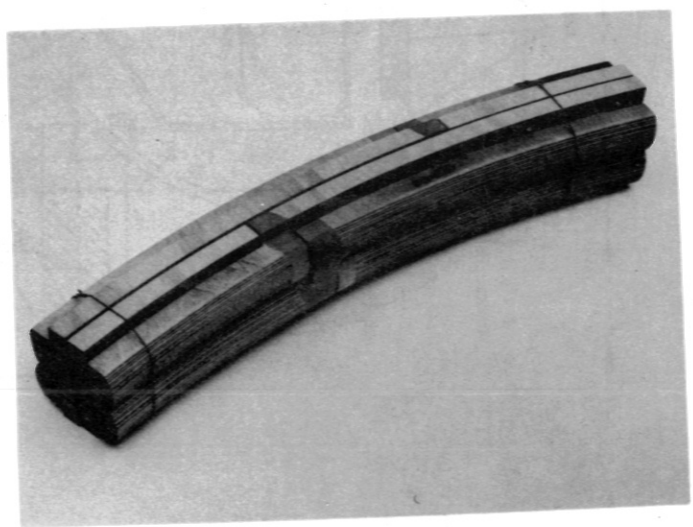

Fig.4: Model of the cross-over section (MP2)

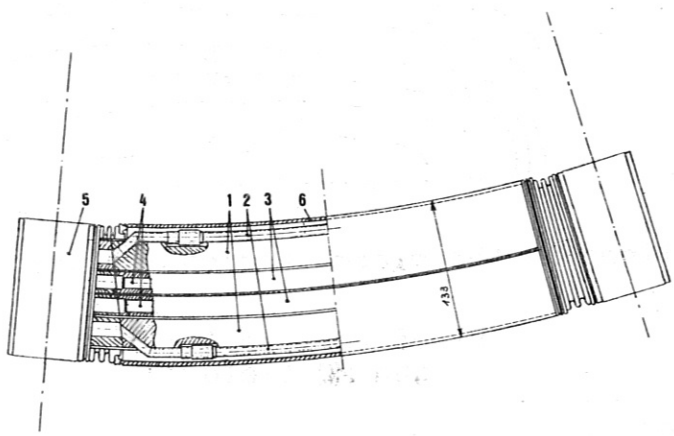

Fig.5: Section of multipole coil 2 with joints between two holders
1 external conductor
2 cooling pipe
3 internal conductor
4 cooling bore
5 holders
6 shield tube

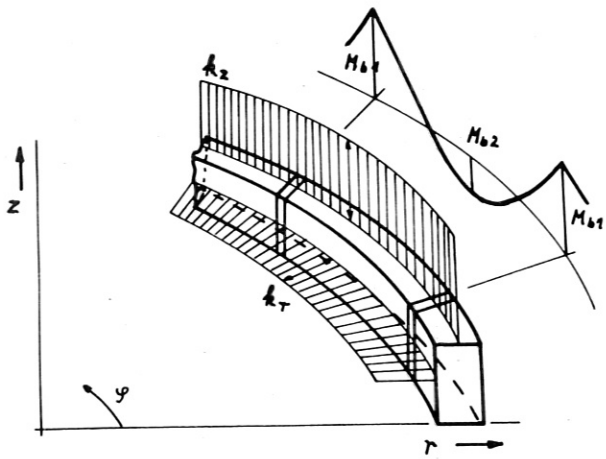

Fig.6: Multipole conductor with typical loads and bendings between two holders
Mb1, Mb2 bending moments
k_R radial line loads
k_Z axial line loads

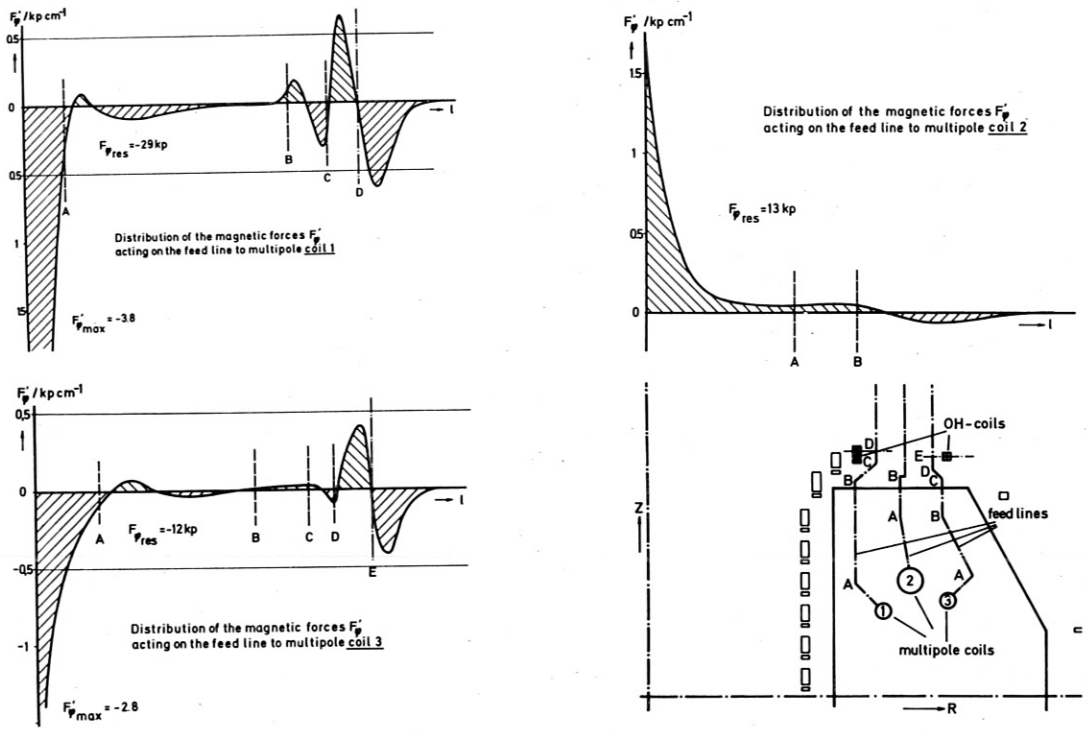

Fig.7: Load of the leads-in

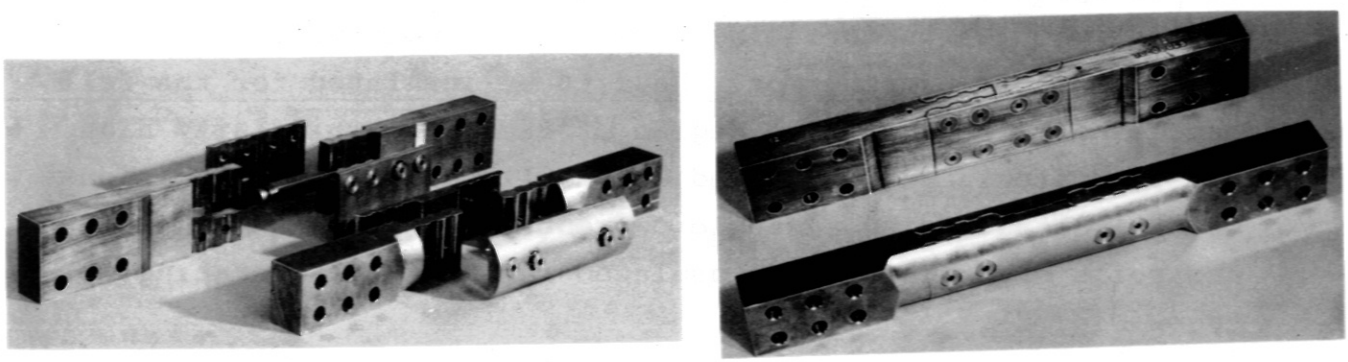

Fig.8: Joints for testing

THE ASDEX OHMIC HEATING ELECTRICAL SYSTEM

H.Preis, H.Wedler

Abstract

A simplified plasma model is used to calculate the plasma current that can be attained with the planned OH system. Since a certain minimum voltage is required for igniting the plasma discharge it is advantageous to switch the discharge resistor to a lower value after ignition, as the calculations show.

1. Technical Concept

The ohmic heating (OH) system for ASDEX is essentially as follows: The OH coils are arranged inside the toroidal field coils, thus affording good coupling (47 %) with the plasma without the use of an iron core. Detachable connections on the OH coils allow the coils to be separated, thus making it possible to divide the OH coils and the whole experiment into two halves. This concept, of course, also involves delicate technical problems since the detachable connections have to be fully capable of taking up the forces resulting from interaction with all axisymmetric coils. Since, moreover, the coils are located in the peak region of the toroidal field, field strengths of up to 60 kG being involved, forces of up to 180 kp/cm are exerted on the leads and cross-overs, i.e. generally on parts deviating from axial symmetry. The connecting joints, furthermore, have to be insulated for the full operating voltage. As the degree of risk is particularly high here, a circuit was developed which allows symmetric division of the voltage using a single current breaker. This means that the coils have only to be insulated for half the operating voltage (Fig. d).

The technical data of this concept have already been reported in a number of papers /1/, /2/. A detailed paper will be published later /3/.

2. Equivalent Circuit

The following equivalent circuit was chosen for the calculations described below (Fig.a):
The coupling with other components was neglected. All elements are introduced as constant quantities. Only for the plasma resistance is a time dependence given, this being described in detail under "Plasma Model". Skin effects and variation of the plasma inductance are neglected.

3. Primary Current and Energy at Constant Plasma Resistance

The following differential equations are valid for the case $r_{p(t)} = \text{const.}$

I $\quad L_{11}i'_1 + L_{12}i'_2 + (R_1 + R_v)i_1 = 0;$

II $\quad L_{12}i'_1 + L_{22}i'_2 + R_p i_p = 0;$

With the boundary conditions: $i_{1(0)} = I_1$ and $i_{2(0)} = 0$ one obtains by means of the Laplace transform the following solutions:

III $$i_1 = \frac{i_{1(0)}}{p_1 - p_2} \left\{ (p_1 + \frac{2}{1 - k^2}) e^{p_1 t} - (p_2 + \frac{2}{1 - k^2}) e^{p_2 t} \right\}$$

IV $$p_{1/2} = \frac{1}{2(1 - k^2)} \left\{ -(\delta_1 - \delta_2) \pm \sqrt{(\delta_1 + \delta_2)^2 - 4(1-k^2)\delta_1\delta_2} \right\}$$

$$k^2 = L_{12}^2/L_{11}L_{22} \qquad \delta_2 = R_p/L_{22} \qquad \delta_1 = (R_1 + R_v)/L_{11};$$

In order to induce a certain plasma current I_p, one requires a primary current

V $$I_1 = \frac{L_{22}}{L_{12}} \cdot \frac{1-k^2}{1} \cdot \frac{p_1 - p_2}{e^{p_1 t^x} - e^{p_2 t^x}} \cdot I_p \text{ with } t^x = \frac{\ln p_1 - \ln p_2}{p_2 - p_1}$$

4. Primary Current, Flux and Energy for the Dynamic Phase

A much more exact estimate of the primary current, the flux and the energy can be obtained by making the following assumptions:
The plasma current $i_p(t)$ rises in the dynamic phase discussed here as $i_p(t) = I_p \cdot t/T$. I_p is the peak value of the plasma current, while T fixes the length of the dynamic phase. For the plasma resistance it is assumed that the relation $r_p(t) \sim T_e^{-3/2}$ is valid for this region. For $T_e(t)$ we assume a linear rise and then we obtain: $r_p(t) = R_o \ (t/T)^{-3/2}$

From eq.II it follows that:

VI $$\Psi_{12} = w_1 w_2 \phi_{12} = L_{12} \cdot i_1 = L_{22} i_2 + \int r_p i_p dt$$

With the assumptions made it is possible to solve the equation:

$$L_{12} I_1 = L_{22} I_p + 0.5 \ R_o \ I_p T$$

With $R_o = 5 \ \mu\Omega$ and T = 50 msec one obtains the following values for ASDEX:

$I_1 = 23$ kA; $W_{1m} = 2.2$ MJ; $\Psi_{12} = 1.93$ Vsec;

The ASDEX OH system delivers $\Psi_{12} = 2.52$ Vs for the dynamic phase.

5. Plasma Model

The estimates made in "Primary current and energy ..." and "Primary current, flux ..." are based on very simple assumptions. Much more accurate results can be obtained by using a detailed plasma model. For the calculations discussed here we took as a basis the following simplified model, our long-term objective being a solution in which the plasma is represented by a suitable code of its own. Our model plasma is developed in three phases:

Phase 0: In the phase 0, starting from a primary electron, a ring voltage induced by the OH circuit is applied to develop an electron avalanche according to the Townsend and streamer mechanism. Up to 300 V and field strenght values of .29 V/cm are available for ignition of the discharge. In this phase the plasma currents are very low, the length of this phase being < 1 ms. It was therefore not taken into account in our calculations.

Phase 1: Phase 0 is followed by phase 1, which can already be diagnosed optically or by simple current measurements. It is assumed that the electron temperature T_e is constant during this time. The electron density and the degree of ionization grow linearly. The plasma resistance accordingly drops with $1/n_e$. As a typical value for this phase we take 5 ms. This time was not varied in our calculations. The initial resistance of the plasma is denoted as $R_{p(to)}$ and the final resistance of this phase as $R_{p(t_1)}$ (see also Fig. b). For r_p it then holds that

$$r_{p(t)} = R_{p(t_o)} \left\{ 1 - \frac{R_{p(to)} - R_{p(t1)}}{R_{p(to)}} \frac{t}{T} \right\}$$

Phase 2: After complete ionization the electron temperature increases, a linear rise being assumed for simplicity. The plasma resistance is determined by means of the equation $r_{p(t)} \sim T_e^{-3/2} / Z_{eff}$. The boundary values of this phase are denoted in our calculations by $R_{p(t1)}$ and $R_{p(t2)}$. The phases 1 and 2 relevant for these investigations are shown schematically in Fig. b. If the values for the electron temperature and Z_{eff} that are expected in ASDEX are taken, the resistance can be determined relatively accurately on the basis of experimental data from Pulsator and TFR. This value can be roughly defined as $10^{-6}\Omega < R_{p(t2)} < 5\ 10^{-6}\Omega$. As we take an electron temperature of 10 eV for $t = t_1$ in our model, we obtain for $R_{p(t1)}$ values between 600 and 3000 $\mu\Omega$.

6. Calculation of Plasma Current

In these calculations the plasma resistance is represented by the schematic curve in Fig.b. The boundary $R_{p(to)}$, $R_{p(t1)}$ and $R_{p(t2)}$ are varied in the individual calculations. The calculations were based on the Netz III program /4/, which was developed for the analysis of transient processes in linear networks.
Figure 1 shows the electron temperature and the plasma resistance for phases 1 and 2. As parameter we took the time t_2 in which the electron temperature attains its final value. Owing to the already quoted relation $r_p = f(T_e)$ the plasma resistance drops very fast to its final value $R_{p(t2)}$ with only weak dependence on t_2. As further calculations showed, this time has a minimum influence on the plasma current. For the following calculations t_2 was given as $t_2 = 50$ ms.

In Fig.2 the plasma current $i_p = f(t)$ is normalized to 500 kA. The plasma resistance at $t = 0$ was varied between 3 and 50 mΩ (curves 2,3 and 4). No influence of the current was detected for times $>$ 5 ms. For comparison, the plasma current for $r_p = 0$ was represented by a dashed curve ($I_p = 675$ kA) and

for r_p = const. = 5 $\mu\Omega$ as curve 1 ($\hat{I}_p$ = 645 kA).
The same variation was performed in Fig.3, but for a different plasma resistance $R_{p(t2)}$. In this case, too, the influence of the initial plasma resistance is slight.

The influence of the plasma resistance at the end of the dynamic phase $R_{p(t2)}$ is shown in Fig.4. The resistance was varied between the limits 0.5 and 10 $\mu\Omega$. The peak currents attainable as a function of the respective resistance are plotted in Fig.c.
In the investigations so far the discharge resistor R_v was not varied (R_v = 0.667Ω). In Fig.5 the results with various discharge resistors are presented. The significant feature of this plot is that the highest plasma current is attained for R_v = 0.34Ω. This is also plausible since very little current is induced in phase 1, as this figure shows. With short break times L_1/R_v a great deal of energy is already dissipated in the resistance R_v during this phase. For R_v = 1Ω already 75 % of the stored energy is dissipated after 5 ms. In Fig.6 the plasma current and the voltage at the plasma $u_p = i_p \cdot r_p$ are represented for various R_v values. As a relatively high voltage is required for ignition of the discharge, the discharge resistor was switched over by an appropriate signal immediately after ignition by an ignitron or spark gap.

This method yields a current of 500 kA. In the meantime another run in which the resistor was switched back to 0.2Ω already after 1 ms has been calculated. The peak plasma current calculated in this case was 570 kA.

7. OH Circuit

The circuit proposed for later operation is to be experimentally tested soon. The voltage load of the coils to ground can be accomplished here by using just one breaking switch S1.

The coils, which are designed for an operating voltage of 20 kV, therefore allow voltage pulses of 40 kV to be generated in theory. In order, however, to reduce the risk as much as possible, the level is set at a maximum of 30 kV for ignition of the discharge, this being equivalent to an open-circuit voltage of 300 V at the plasma.

8. Current and Voltage Waveforms after Breaking the OH Current

To achieve further optimization of the OH circuit as a means of sparing the breaker, the current and voltage waveforms were calculated with the Netz III program. The circuit for this investigation is presented in Fig.e. A capacitor bank with 0.625 mF produces current zero in the breaker S1. The break time is marked in Fig.7 and 8. Figure 7 shows the current and voltage without the use of an inductor. In Fig.8 the breaker is additionally protected with an inductor. In this case the phase with low current is increased by a factor of two. These calculations have been made so far with an ideal breaker, i.e. for times $t \geq t_s$ the current in the breaker will be better adapted to real conditions by a transition function.

References

/1/ R.Allgeyer et al., ASDEX, A Tokamak with Axisymmetric Divertor, Proc.8th Symp. on Fusion Technology, Jutphaas 1974, p. 317.

/2/ R.Allgeyer et al., The Design of the ASDEX Tokamak, Proc.6th Symp. on Engineering Problems of Fusion Research, San Diego 1975, p. 378

/3/ G.Klement et al., Technical Problems of the ASDEX OH System (to be published)

/4/ H.Preis, Die Analyse transienter Vorgänge in
Report IPP 4/87 (1971).

Table I

Datas of ASDEX OH System

Number of coils	2 x 12
Number of turns	100
Max.Operating voltage	30 kV
Voltage at the plasma	300 V
Coupling to the plasma	47 %
OH coil inductance L_{11}	8.4 mH
Plasma inductance L_{22}	3.7 µH
Mutual inductance L_{12}	84.2 µH
Coil resistance R_1	15 mohm
Coil current	30 kA
Current density	31.7 A/mm^2
Temperature rise	15° C
Charging time	0.5 s
Flat top time	5 s
Discharging time	10 - 100 ms
Total energy in the coils	3.8 MJ
Flux swing for dyn.phase	2.5 Vs
Flux swing for flat top	2.5 Vs
Axial force per coil	32 to
Tensile force per turn	2 to
Inductive flux	1.85 Vs
Resistive flux (dyn)	0.8 Vs
Resistive flux (flat top)	2.5 Vs

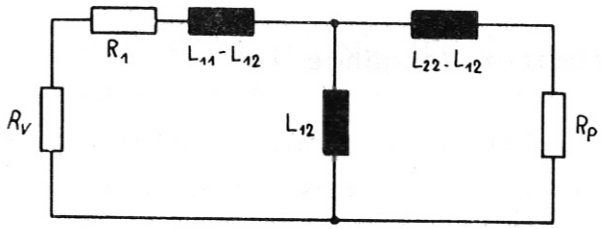

Fig.a: Equivalent circuit for the OH-system with plasma

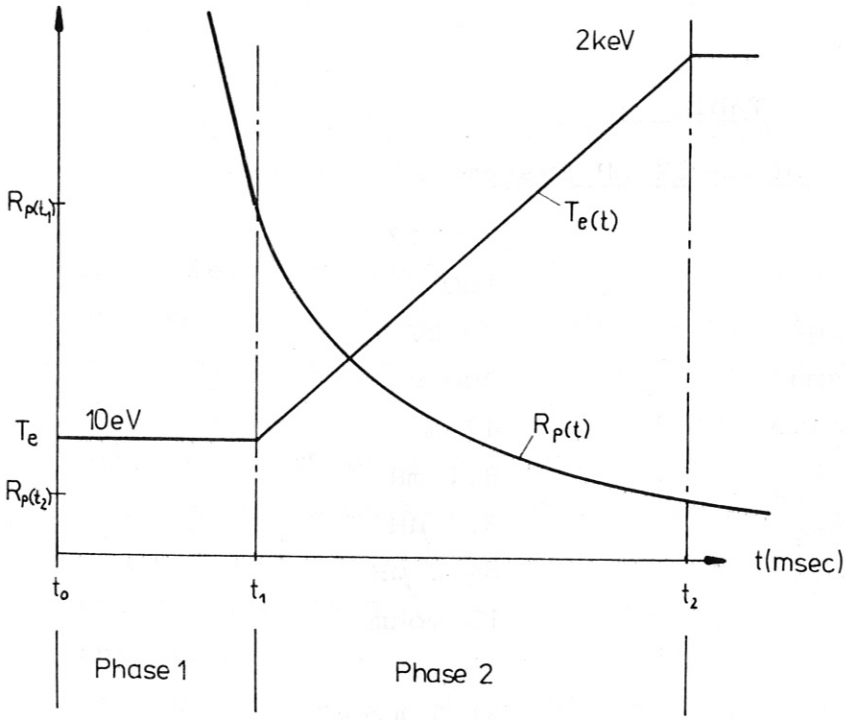

Fig.b: Schematic representation of the electron-temperature and the plasma resistance for phase 1 and 2

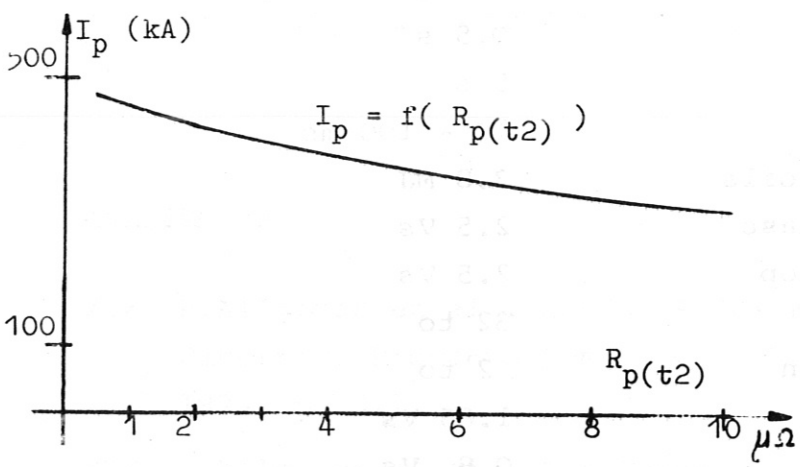

Fig.c: Peak plasma current I_p as a function of the plasma end resistance $R_{p(t2)}$

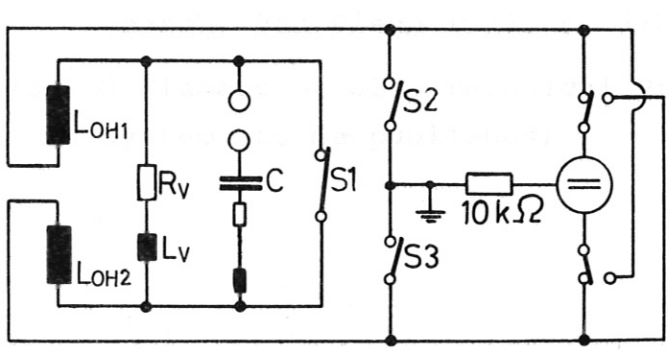

Fig.d: Equivalent circuit for the ASDEX-OH-System

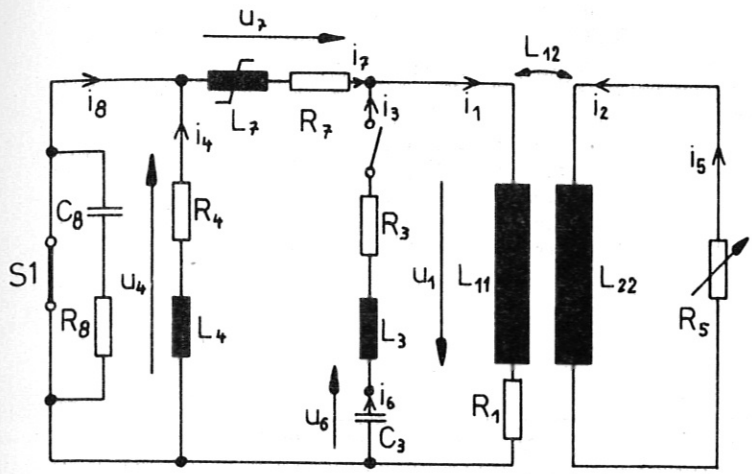

Fig.e: Equivalent circuit for calculation of the current and voltage wave forms in the OH-System

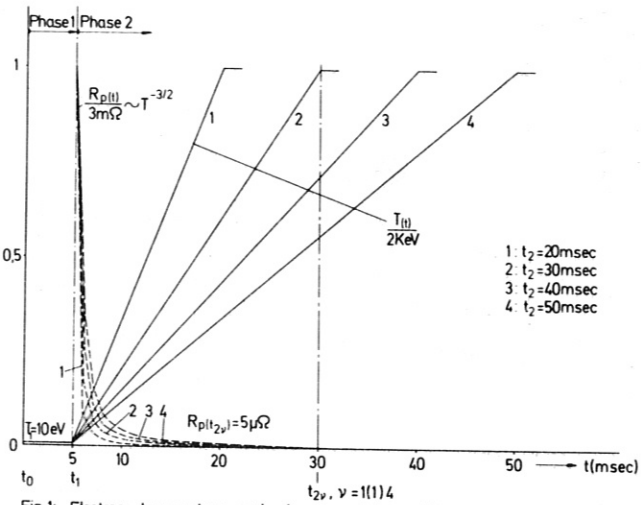

Fig.1: Electron temperature and plasma resistance $R_{p(t)}$ versus time at different temperature rise times

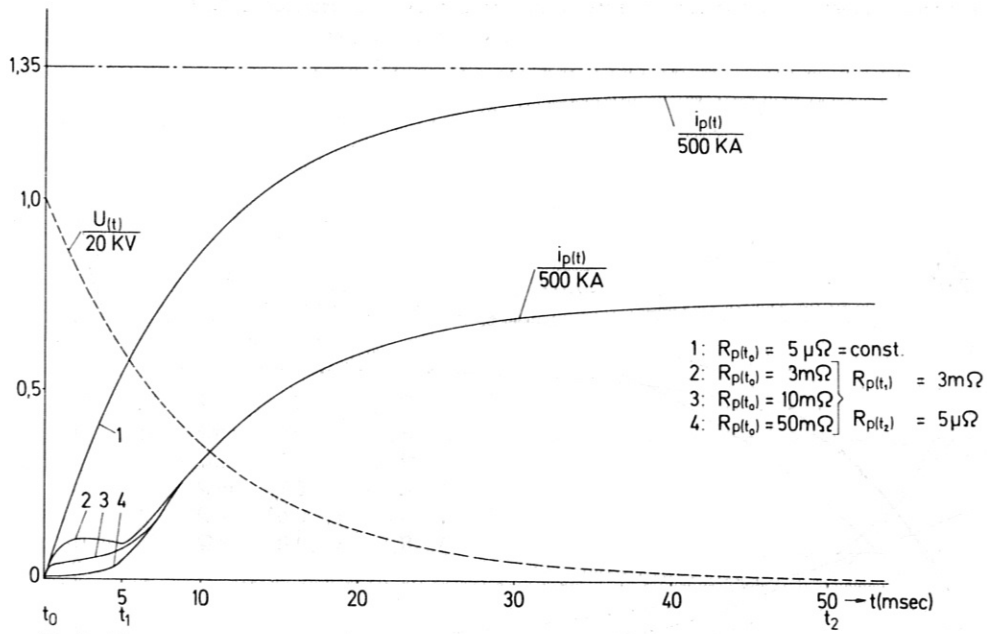

Fig. 2: Plasma current versus time with initial plasma resistance $R_{p(t_o)}$ as the parameter $R_{p(t_2)}$ = 5μΩ

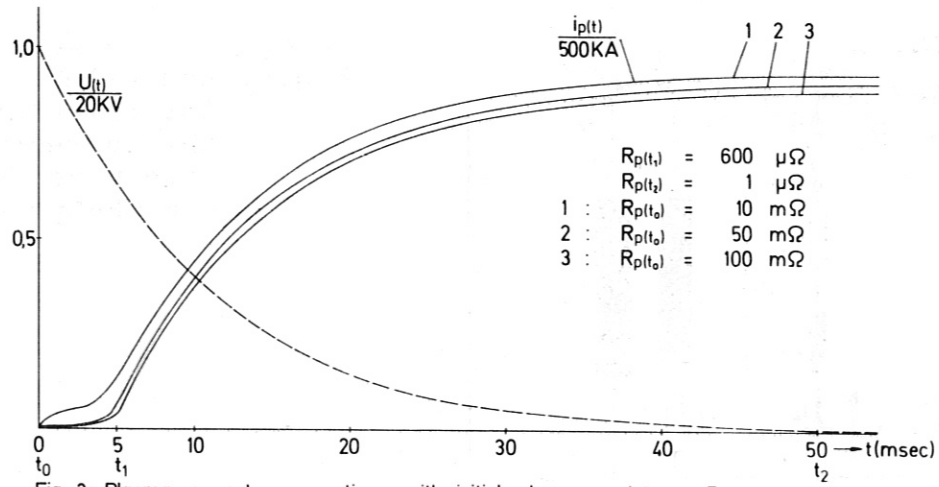

Fig. 3: Plasma current versus time with initial plasma resistance $R_{p(t_o)}$ as the parameter. $R_{p(t_2)} = 1\,\mu\Omega$

$R_{p(t_o)} = 50\ m\Omega$

	$R_{p(t_1)}$ [mΩ]	$R_{p(t_2)}$ [µΩ]
1	0,3	0,5
2	0,6	1
3	1,2	2
4	3	5
5	6	10

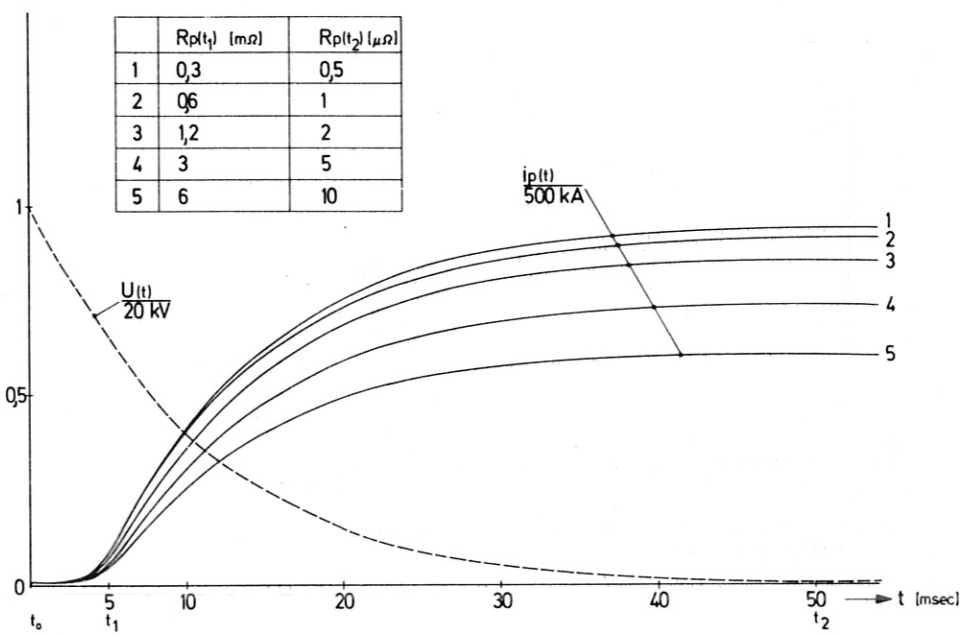

Fig. 4: Plasma current as a function of time with the end plasma resistance $R_{p(t_2)}$ as the parameter

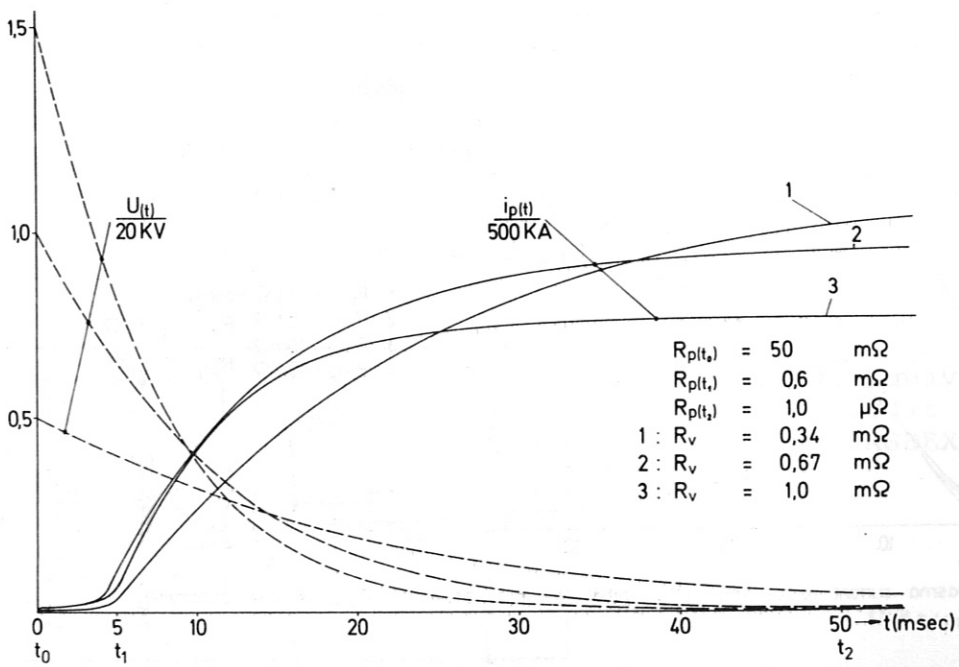

Fig. 5: Plasma current versus time with discharge resistor R_v as the parameter

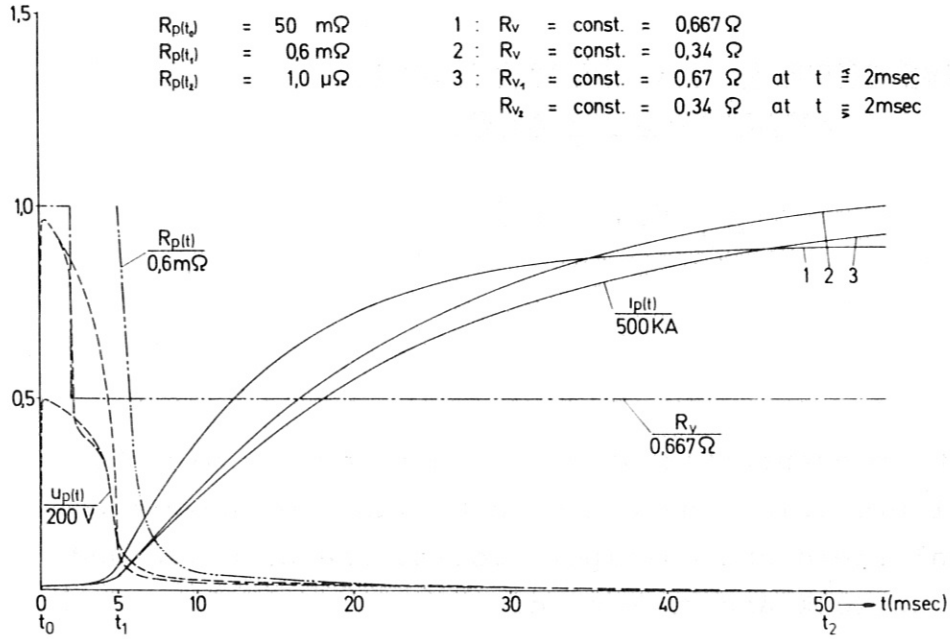

Fig. 6: Plasma voltage $u_{p(t)}$ and plasma current $i_{p(t)}$ versus time with different discharge resistors R as the parameter. Curve 3 represents calculations with a time variable discharge resistor.

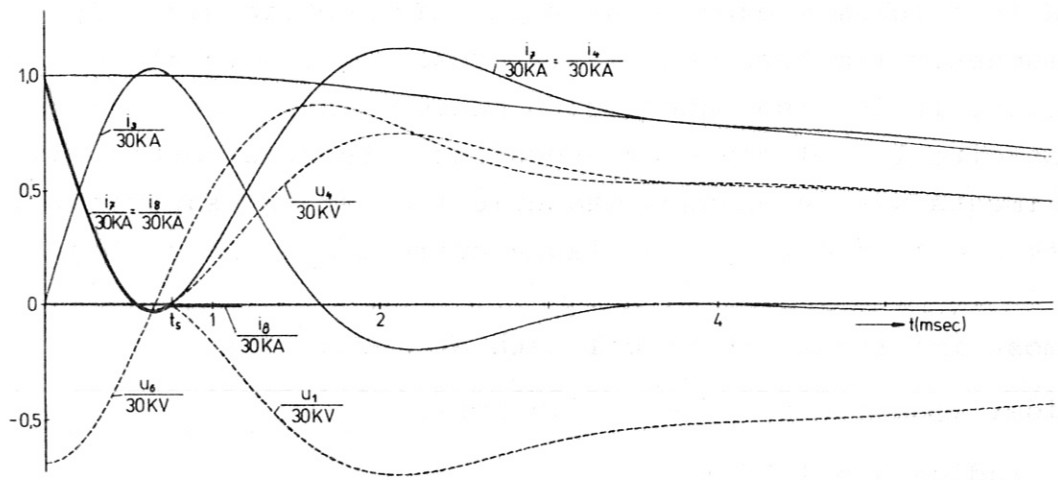

Fig. 7: Current and voltage when breaking without inductor

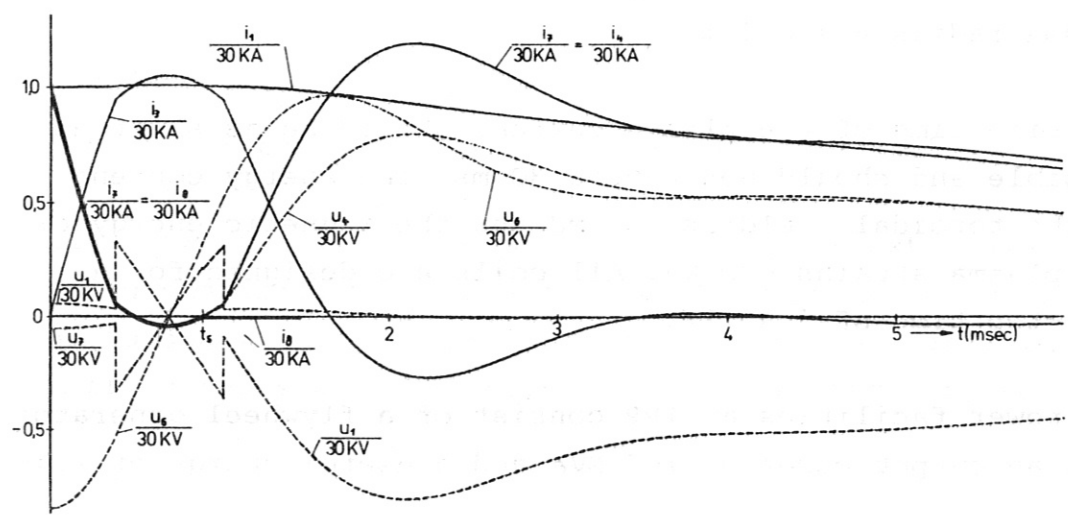

Fig. 8: Current and voltage when breaking with inductor

THE POWER SUPPLY FOR THE POLOIDAL FIELD COILS OF ASDEX

H.Rapp, F.Gresser

Abstract

Owing to the present lack of sufficient power sources at IPP special provisions have had to be made for powering the vertical field and multipole coils. The solution and the future outlook are presented.

1. Introduction

ASDEX is a Tokamak experiment with axisymmetric divertor and magnetic limiter. The plasma cross-section is almost circular. It is also intended to conduct investigations on non-circular plasma cross-sections without divertor and experiments with a opening magnetic limiter for suppressing the skin effect during the plasma current rise phase(Fig.1)/1/.

The most important electrical data of ASDEX are:

Toroidal magnetic field B_T = 2.8 Tesla

Major radius R = 1.67 m

Plasma current (typical) I_p = 500 kA

Plasma radius a = 0.4 m

The rise time of the plasma current should be as short as possible and should not exceed 30 ms. The energy content of the toroidal field is 230 MJ and the magnetic energy of the plasma attains 600 kJ. All coils are designed for a flat-top time of 5 s /2/.

The power facilities at IPP consist of a flywheel generator with an output power of 167 MVA and a useful energy of 1.45 GJ

/3/ and a small flywheel generator with an energy content of 15 MJ. The large generator powers the toroidal field coils via a diode rectifier. The small generator is used for exciting the ohmic heating transformer via a mercury vapour static converter. Both generators are fully loaded. Only some energy is left and in the case of the large generator it is possible to raise the reactive current load. Using power from the mains is out of the question in view of the low shooting sequence permitted.

The planning of the ASDEX experiment was therefore subject to the subsidary constraint that no independent source is available for the time being to control the currents of the vertical field coils and multipole coils. The present state of the ASDEX power supply is shown in Fig.2. The future extensions are indicated by dotted lines.

2. Vertical Field Powering

The vertical field coils are connected in series with the toroidal field coils. The latter act as a powerful constant current source with a time constant of 3.5 s compared with the 0.4 s transient response of the exciting field of the flywheel generator. The current in the vertical field coils is controlled with a variable shunt /4/.

For this purpose three alternatives were put forward:

A. DC chopper

B. Self-controlled static converter system

C. Generator controlled shunt converter (Fig.3).

The first two possibilities are independent of external sources. The third possibility assumes that an AC voltage source which can be loaded with at least reactive current is available for controlling the static converter. A suitable facility for this

purpose is the 1.45 GJ flywheel generator. This was confirmed by having the manufacturer test the generator load.

A serious disadvantage of the self-sufficient solutions is that the requirement of the current impressing high energy toroidal magnetic field would severely hamper the commissioning work and trials. In contrast, the alternative with a generator controlled shunt converter also works without current impression. The vertical field coils can be powered in the usual way if the experimental data and hence the generator load are reduced and the polarity is reversed.
The advantage of the shunt converter circuit as regards the generator load is particularly pronounced for $i_V \approx i_H$ when the converter direct current becomes zero. The circuit also allows a short-time reversal of the current in the vertical field coils, which may be interesting for modifying the initial conditions for plasma ignition and palsma current rise. In the event of overvoltages at the vertical field coils as a result of plasma disruption, a current passes through the rectifier valves in the forward direction.
A disadvantage of the shunt converter is the static coupling of the open-circuit voltage to the main field current via the generator voltage. In view, however, of the narrow margin of tolerance towards smaller values of the toroidal field and the necessity of sufficiently high q-values of the plasma this disadvantage seems to be of minor significance. In addition, the transmission ratio of the rectifier transformer can be matched. The reaction on the main magnetic field is the same in all proposals. It is negligibly small.

Despite the high costs for the 400 m long power line and the rectifier transformer that are needed ,the alternative with shunt converter is more favourable by reason of the operational advantage and the reliability of the technique. It will serve as an intermediate possibility until another new flywheel generator is available. The installations will then

become part of a large flexible static converter unit with connections to all large experiments at the IPP. The static converter will consist of two modules, each with a three-phase bridge circuit with a rated current of 22.5 kA for a current flow time of 5 s. The open-circuit voltage is a maximum of 1200 V. Owing to the long power line the inductive and ohmic voltage drops are relatively high. They are $d_x = 0.16$ and $d_r = 0.13$. Each of the two modules works in 6-pulse mode, or together 12-pulse mode. The rectifier transformer is designed for a rated frequency of 100 Hz and a continous power of 17 MVA. The pulse factor is 3.3. The transformer has two primary windings, each of them for a phase voltage of 2.75 kV. They can be connected in series for 10 kV operation as soon as new flywheel generator is available.

Figure 4 represents the simulation of the plasma current rise phase. The voltage excess of the vertical field converter reaches about 50 %, which is required as an amplification reserve for the feedback loop for plasma stabilization. A current of 45 kA in the vertical field coils can stabilize a plasma with a current of approximately 650 kA.

3. Multipole Current Control

The multipole coils will also be connected in series with the toroidal magnetic field coils and provisionally operated in the steady-state mode. Auxiliary coils will be used to compensate the residual field in the plasma region. Experiments with elongated plasma cross-sections call for controllable multipole coils. For this purpose two converter modules of the same type as for the vertical field will later be available. In the event of reduced experimental parameters one of the two converter modules intended for the vertical field can be used to control the multipole field. This is possible both in the shunt mode as in the case of the vertical field and in the usual type of circuit.

For vertical elongation a current with the same direction as the plasma current is passed through the middle multipole conductor. The smaller multipole conductors are connected in series and short-circuited, thus affording passive vertical stabilization of the plasma (Fig.5). If necessary, passive stabilitzation can be replaced by active stabilization with a less powerful amplifier. The middle multipole conductor carries a maximum current of 8 x 45 kA = 360 kA. This yields an elongation of the plasma of 1.8 at a plasma current of 500 kA.

4. OH Transformer Power Supply

The OH coils are charged by a 15 MJ flywheel generator with mercury rectifier. The current attains its final value of 30 kA within 0.5 s. This corresponds to a flux swing of 2.4 Vs. The energy of at least 5 MJ remaining in the generator can be used for flux reversal during the flat-top time and hence for maintaining the plasma current. The low permissible effective current of the antiparallel valves constitutes another restriction at first. Later a reversing thyristor static converter with an apparent power of 2 x 25 MVA will be made available to eliminate these restrictions. This should make it possible to maintain a plasma current of 500 kA for 5 s, provided the energy confinement time of the plasma is 0.4 s. Simultaneous excitation of the vertical field coils for stabilizing the plasma contributes about 10 % of the plasma current during the rise phase.

5. Radial Field Control

Besides stabilizing the plasma in the midplane, the radial field should also allow rigid displacement of the plasma by a few centimeters up or down in order to influence the thickness of the scrape-off layer leading into the divertor. For this purpose a maximum coil current of $\pm$ 2 kA and a peak

power of about 2 x 100 kW are sufficient. In contrast, the experiment with the opening magnetic limiter during the plasma current rise of about 30 ms calls for a current of at least 10 kA.

Measurements on a vessel model including the metal separating sheets between the plasma and the divertor chamber have shown that the radial field is not damped in the plasma region. The field is sufficient to achieve a vertical displacement of the plasma by about 16 cm within a period of 5 ms (Fig.6). Power will be provided by a push-pull amplifier and a capacitor bank with an energy content of approximately 50 kJ. The discharge current of the capacitor for the experiment with opening magnetic limiter will be programmed by means of the charge voltage and a variable resistor. The amplifier is transistorized since the mean radial field direct current in the normal case is zero and static converters show maximum ripple in this respect. Decoupling of the amplifier from the capacitor bank is accomplished with a diode and a thyristor.

References

/1/ K.U.v.Hangenow, K.Lackner, 7th Europ.Conf.on Contr. Fusion and Plasma Physics, Lausanne 1975

/2/ R.Allgeyer, et al., 6th Symp. on Engineering Problems of Fusion Research, San Diego 1975, p. 378

/3/ A.Knobloch, et al., 8th Symp.on Fusion Technology, Jutphaas 1974

/4/ H.Rapp, F.Gresser, Report IPP III/20, 1976

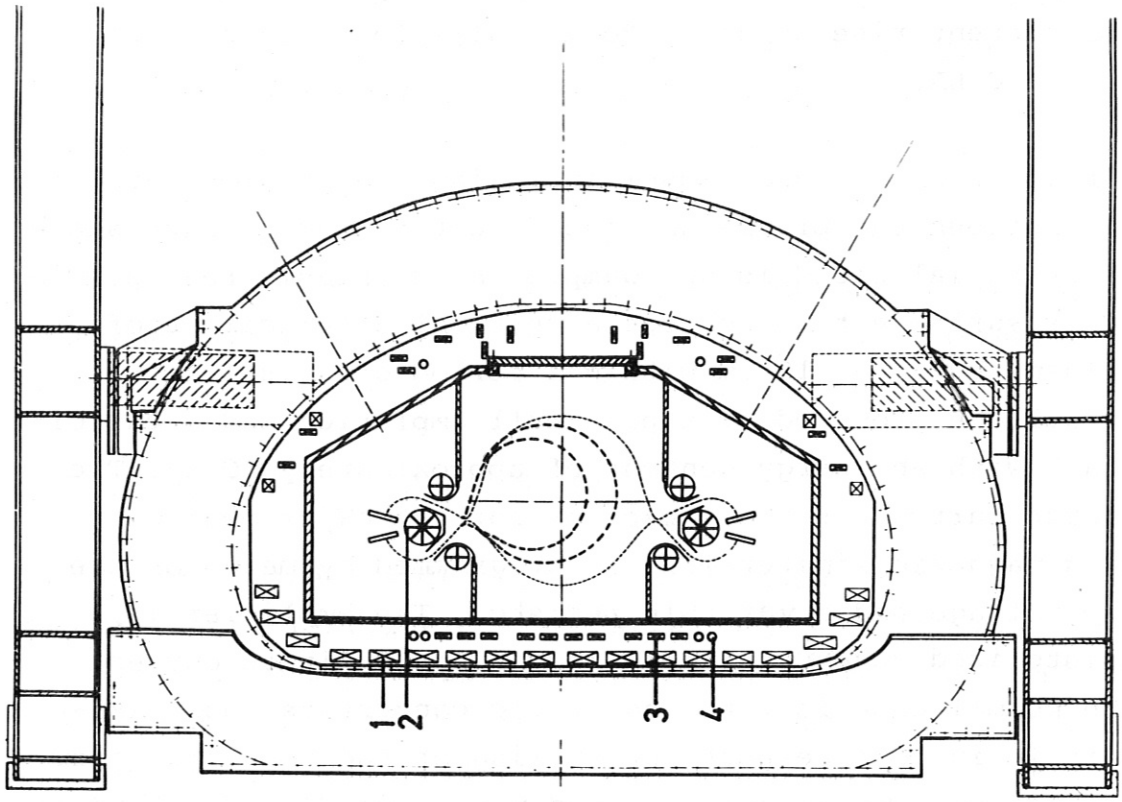

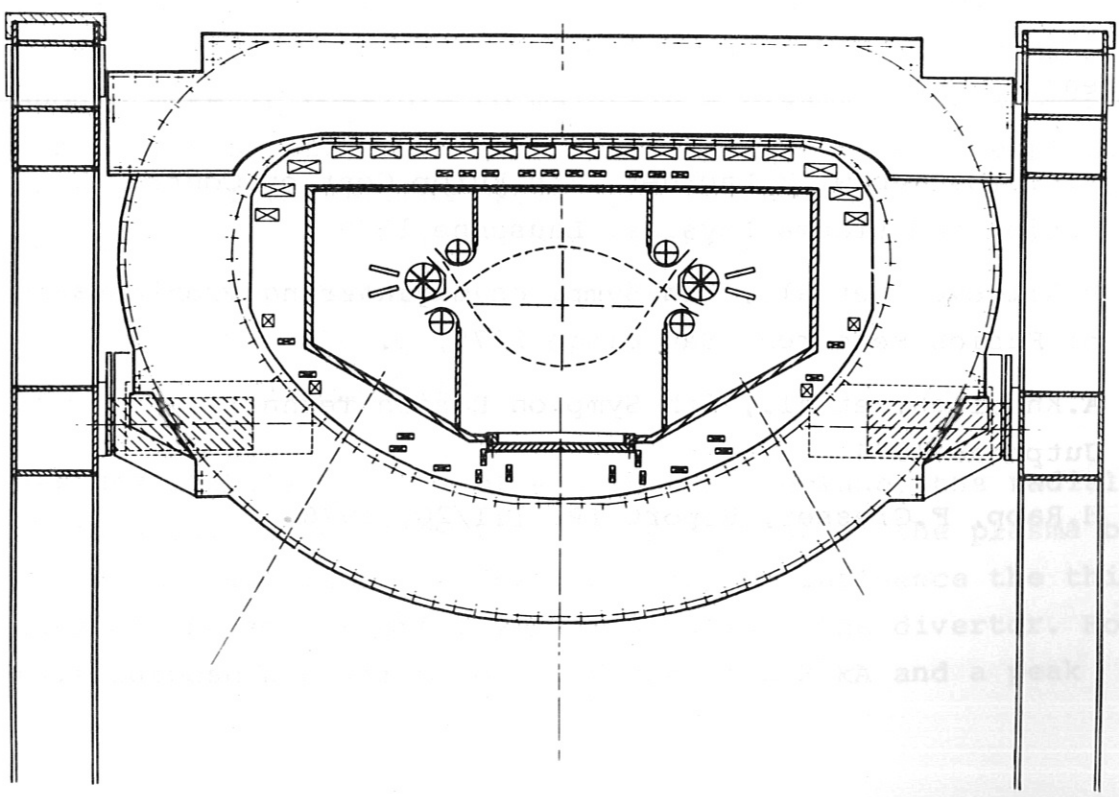

Fig. 1 Several Operating Modes of ASDEX

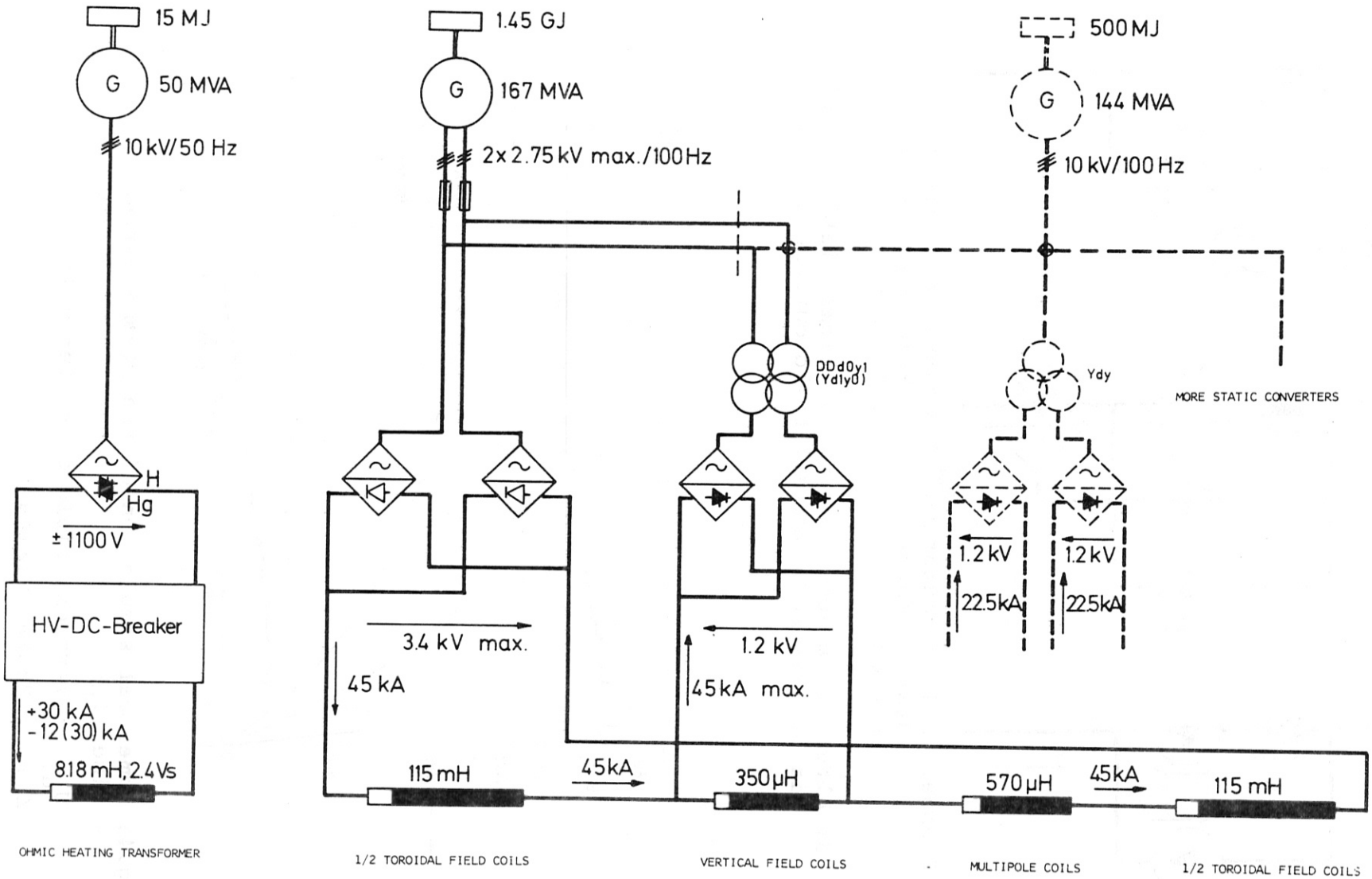

Fig. 2 Power Supply of the ASDEX Coils

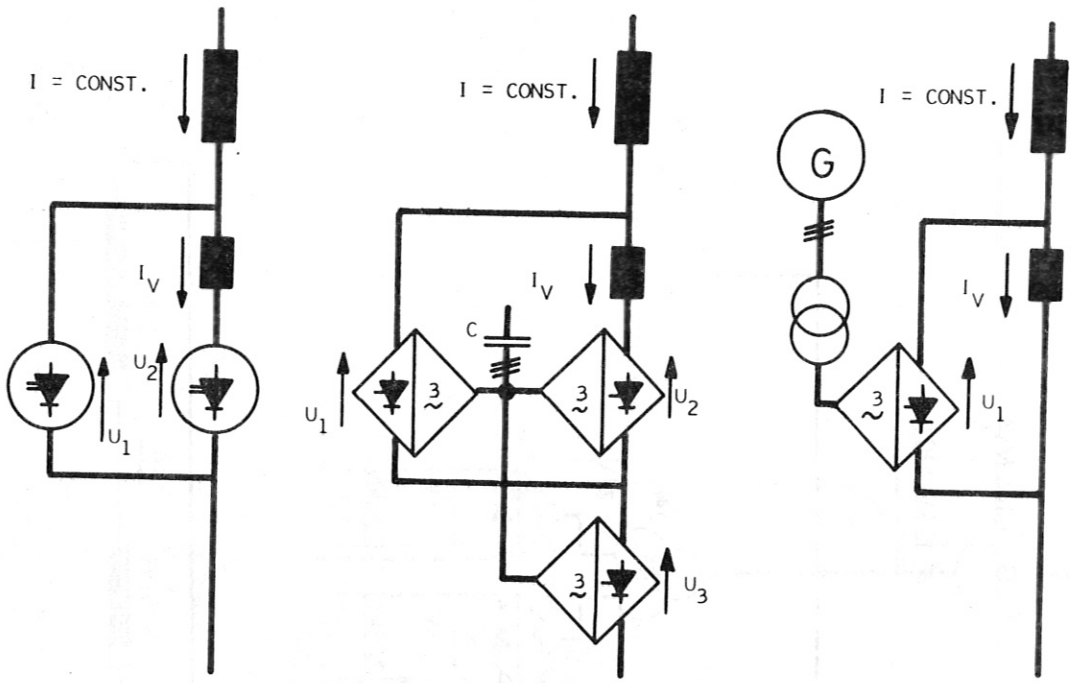

DC-Chopper

Self commutating static converter system

Generator controlled static converter in shunt mode

Fig.3: Alternative solutions for vertical field control via by-pass and toroidal field current source

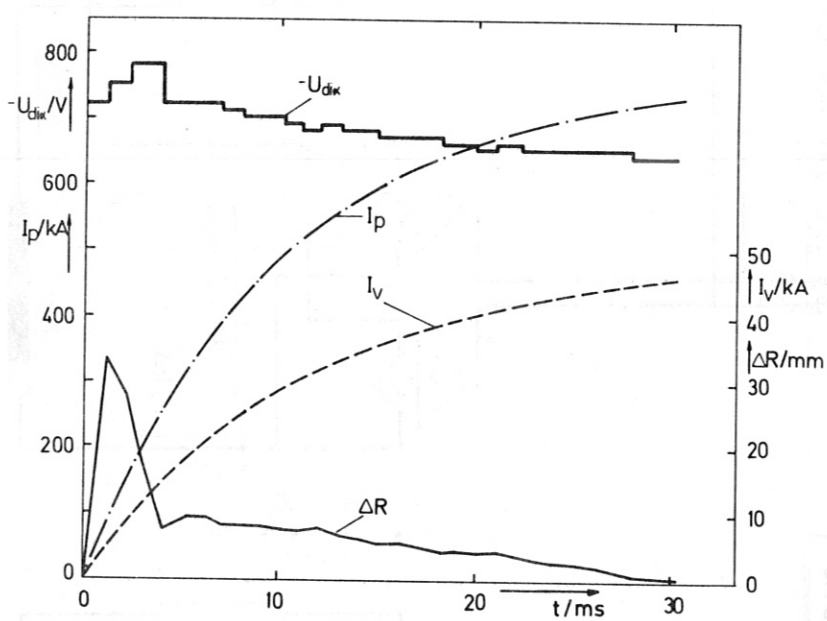

Fig.4: Numerical simulation of the plasma current rise (I_p).

U_{di} : Vertical field converter voltage

ΔR : Radial plasma shift

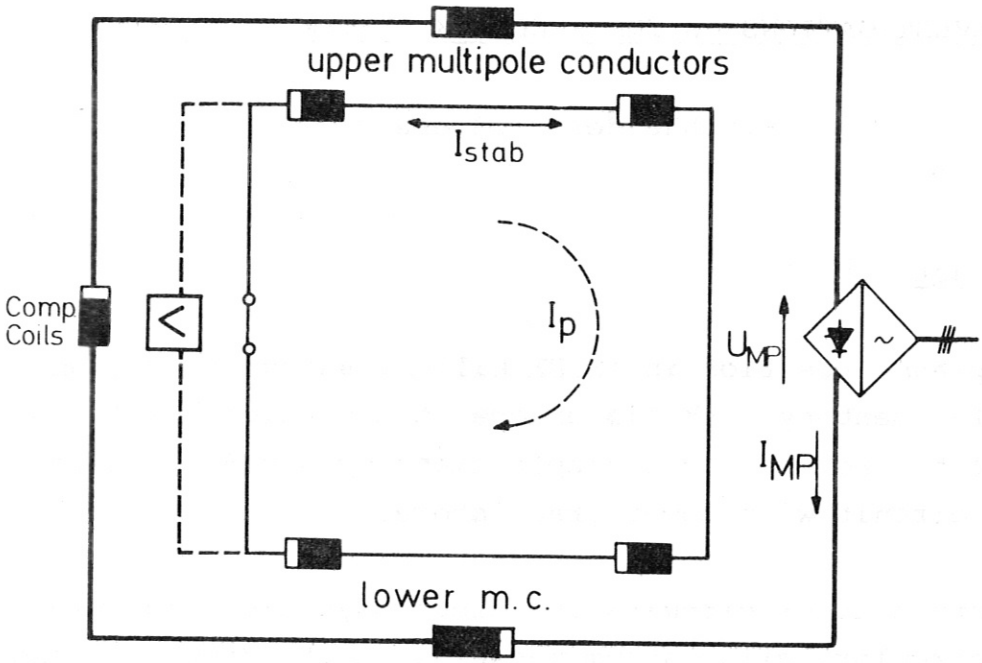

Fig.5: Multipole circuit for elongated plasma cross-section

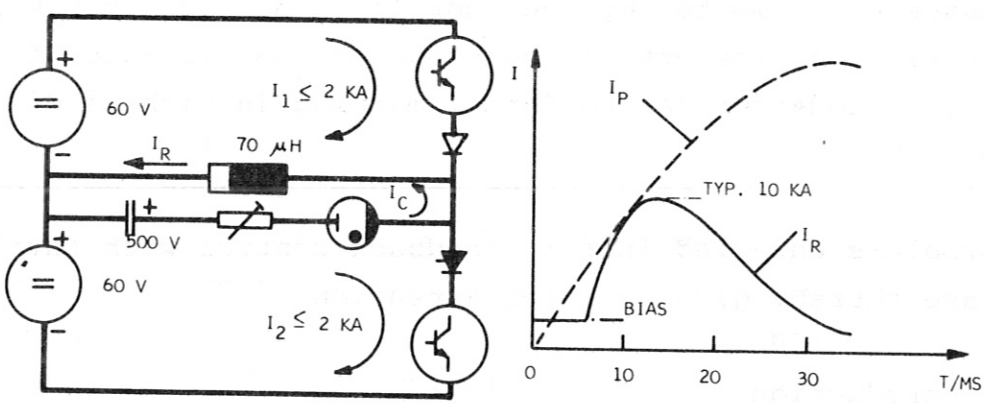

Fig.6: Radial field power supply

INVESTIGATIONS ON THE FEEDBACK SYSTEM OF ASDEX

F.Schneider, F.Gresser

Abstract

The plasma position in ASDEX will be safeguarded from radial displacement by a thyristor-operated vertical field control circuit, from vertical displacement by a radial field control circuit with power transistors.

In both control circuits the electrodynamic properties of the non-circular, slit vacuum vessel with its divertor inserts play a big role. The essential magnetic couplings and time constants were therefore determined in a model of ASDEX.

These dynamic properties and the inter-related plasma physics are represented by means of feedback technology. The control processes are computed by the root locus method and Laplace transformation. For optimizing purposes, use is made of graphic methods such as conformal mapping in Nichols diagrams.

The problems entailed in fast feedback control with thyristors are thereby given special attention.

1. Introduction

The stability of the plasma position in a tokamak depends on a number of effects. For optimum application of an automatic controller it is necessary to investigate these relations according to their quantitative and time behaviour. Roughly speaking, these influences can be divided into passive (dynamic and static) and active (programmed Fig.1/8) and feedback controlled (Fig.1/7) effects.

2. Passive Feedback

Since the use of copper shells is not intended in ASDEX, dynamic, passive stabilization is relatively small. Nevertheless, the induction currents in the vacuum vessel (Fig.1/20), and vertical field coil (Fig. 1/10) cannot be neglected. As the current distribution in the slit vacuum chamber with its divertors is difficult to calculate mathematically, we made a 1 : 10 model of ASDEX (Fig.9). This allowed the magnetic coupling (Fig. 1/23), time constants (Fig. 1/11,21), induction currents and dynamic field distortions to be determined.

A passive influence is also exerted by the vertical field gradient (Fig.1/5) as well as by the laws of poloidal (Fig.1/3) and toroidal (Fig.1/2) flux conservation. In first approximation these are time independent and can be taken together to yield an effective plasma equilibrium (Fig.2/6) /1/.

3. Active Feedback

The active part of the control circuit acts via the vertical field coil (Fig.1/12) with a time constant of 150 ms. The acting time, however, may not exceed 5 to 10 ms. This yields a minimum open loop gain of $G > 15$. The vessel with an approximate time constant of 10 ms (Fig.1/22) causes a delay of second order. Consequently feedback from inside the chamber cannot be achieved with optimum results by means of a simple proportional controller (Fig.3).

There are various methods of investigating control circuits. Besides numerical solution of the differential equation by means of matrices /2/ /3/, there are graphic methods such as the investigation of Bode plots or the root locus method /4/ /5/. With Nyquist and Nichols diagrams /6/ it is additionally possible by conformal mapping to prepare trans-

formation charts, with which test values, e.g. from a model, can be directly evaluated and the appropriate controller for the purpose can be found.

As an example with a PD controller /5/ of the type successfully used in the Pulsator tokamak at Garching /7/ it is possible to achieve an essential improvement of the above behaviour (Fig.4). With a PJPD controller some properties might become even more favourable (Fig.5).

4. Feedback with Thyristors

Our deliberations so far have been based on the assumption of linear amplifiers in ASDEX. For the vertical field in ASDEX, however, thyristors are used /8/. To study this critical amplifier element, we built a model with thyristors and simulated ASDEX elements (f_{gen} = 50 Hz instead of 100 Hz). The oscillograms (Fig.11...13) show for the vertical field coil with chamber as an example the effect of a current return such as is often used in industrial cascade control circuits for shortening the coil time constant. With an increased loop gain, to reach velocities such as are required in ASDEX, there is undesirable overswing (Fig.12,13).

There are various theories for calculating such dynamic properties of a thyristor element in the control circuit /9/,/10/,/11/,/12/. Some are mutually contradictory and none affords a clear and satisfactory method of explaining and eliminating the above phenomenon. We have therefore tried to develop a method by which thyristor control circuits can be relatively easily optimzied up to very high velocities.

If the modulated thyristor voltage is divided into frequency components it is interesting to note that the modulation frequency is not subject to phase shift (Fig.6). There is,

however, superpositioning of the lower side band of the thyristor frequency $f_T = 600$ Hz and the modulation frequency f_M (Fig.7). Of these sub-harmonics ($f_M = f_T = nf_M$) only the first ($f_M = 300$ Hz) plays a role at low modulation and in practice since the amplitude of the higher sub-harmonics (200 Hz, 150 Hz...) is low relative to that of the modulation frequency.

The transmission function of the ASDEX thyristor circuit in conjunction with the vertical field coil can be represented in the Laplace domain as shown in Fig.8. In this way, it can be investigated like any other control circuit with, for example, the deviation chart of the reference chart. It can be seen that the tenfold loop gain causes no overswing (Fig.11), while above a hundredfold gain we have to expect 4 % overswing (Fig.12) and even more (Fig.13). This effect is more or less present, depending on the onset time of the disturbance with references to the phase of the thyristor.

Conclusion

With the afore-said facilities it is possible to describe and optimize the entire control circuit including the plasma, the vacuum vessel and the thyristor amplifier.

References

/1/ V.S.Mukhovator, V.D.Schafranow; Moskow "Plasma Equilibrium in a Tokamak", Nuclear Fusion 11/71, p.605

/2/ J.M.Bailey et al., Oak Ridge, Tennessee "Feedback Control for Plasma Equilibrium in ORMAK", ORNL-DWG-75-9441

/3/ J.Hugill, A.Gibson; UKAEA Culham "Servo Control of Plasma Position in CLEO-Tokamak", CLM-P 382 (1974)

/4/ Gille, Pelegrin, Decaulne; Paris "Theorie et Technique des Asservissements" Dunod Paris (1956)

/5/ W.Oppelt; Darmstadt "Kleines Handbuch technischer Regelvorgänge", Verlag Chemie (1972)

/6/ James, Nichols, Phillips; Cambridge, "Theory of Servomechanisms" Dover (McGraw Hill) New York (1956)

/7/ R.Ammer, et al., IPP Garching,"Feedback-Regelung der Gleichgewichtslage des Plasmas im PULSATOR" IPP internal report.

/8/ H.Rapp, F.Gresser; IPP Garching,"Magnetic Field Control with Constant Current Source and Shunt Voltage Source in the Case of ASDEX", IPP III/20

/9/ J.H.Nizol; CERN Genève "An Investigation into the Use of Programmed Thyristor Controlled Power Supplies for the Pole-Face Windings of the 28 GeV Proton Synchrotron of CERN", MPS/SR/Note 73/42 (1973)

/10/ J.Hugel; Universität Stuttgart "Die Berechnung von Stromrichter-Regelkreisen", Archiv für Elektrotechnik 4/1970 , p.224

/11/ D.Schröder; TH Darmstadt "Grenzen der Regeldynamik von Regelkreisen mit Stromrichter-Stellgliedern", Regelungstechnik und Prozeß-Datenverarbeitung 21/1973, p.322.

/12/ R.Prajoux, P.Thierry, J.Jalade; Lab.du CNRS Toulouse "A Compensation Method for Thyristor Rectifier Control Loops", IFAC-Conference 1974, Proc.I, p.71.

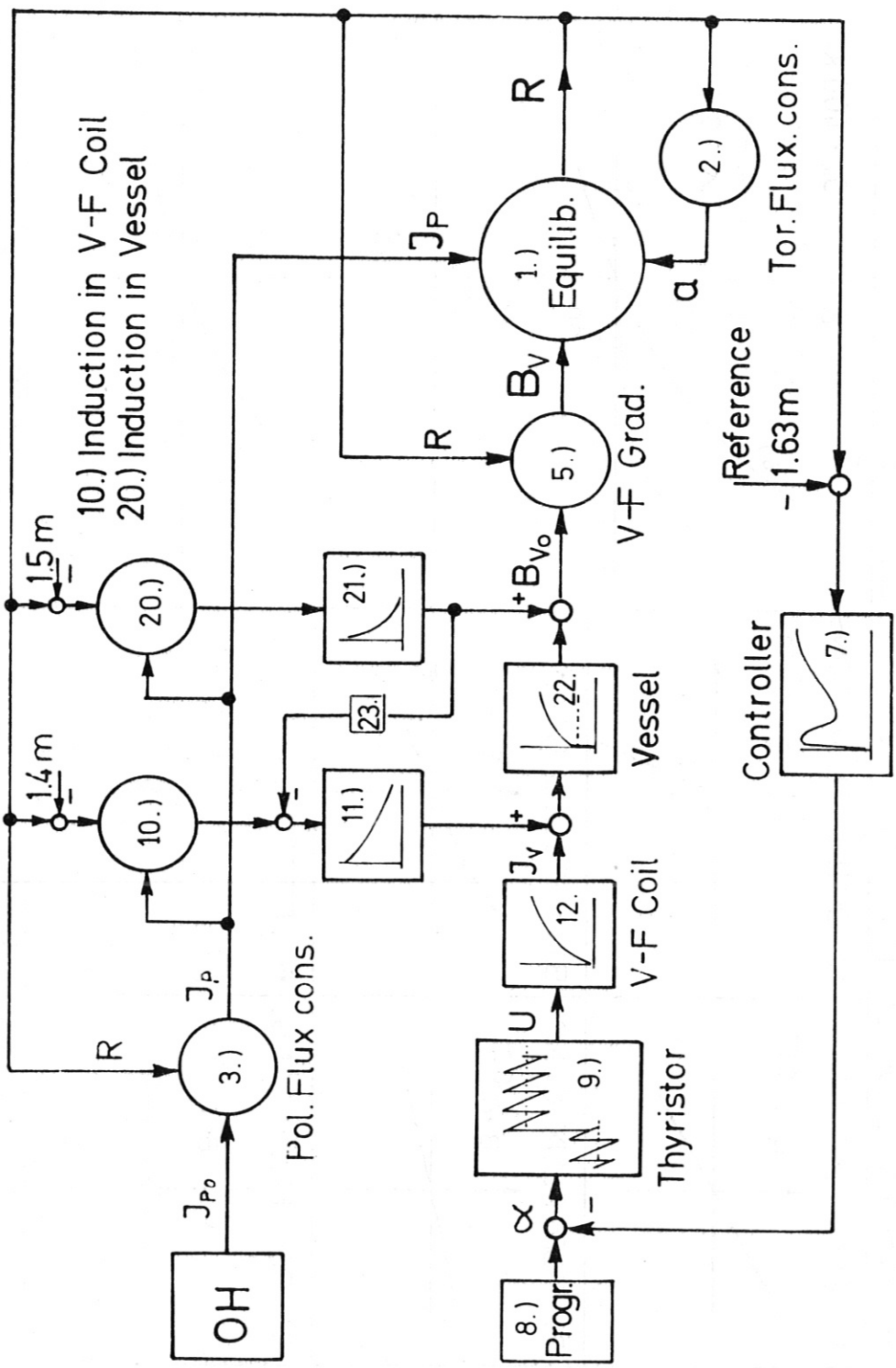

Fig. 1 / V-F Feedback circuit ASDEX

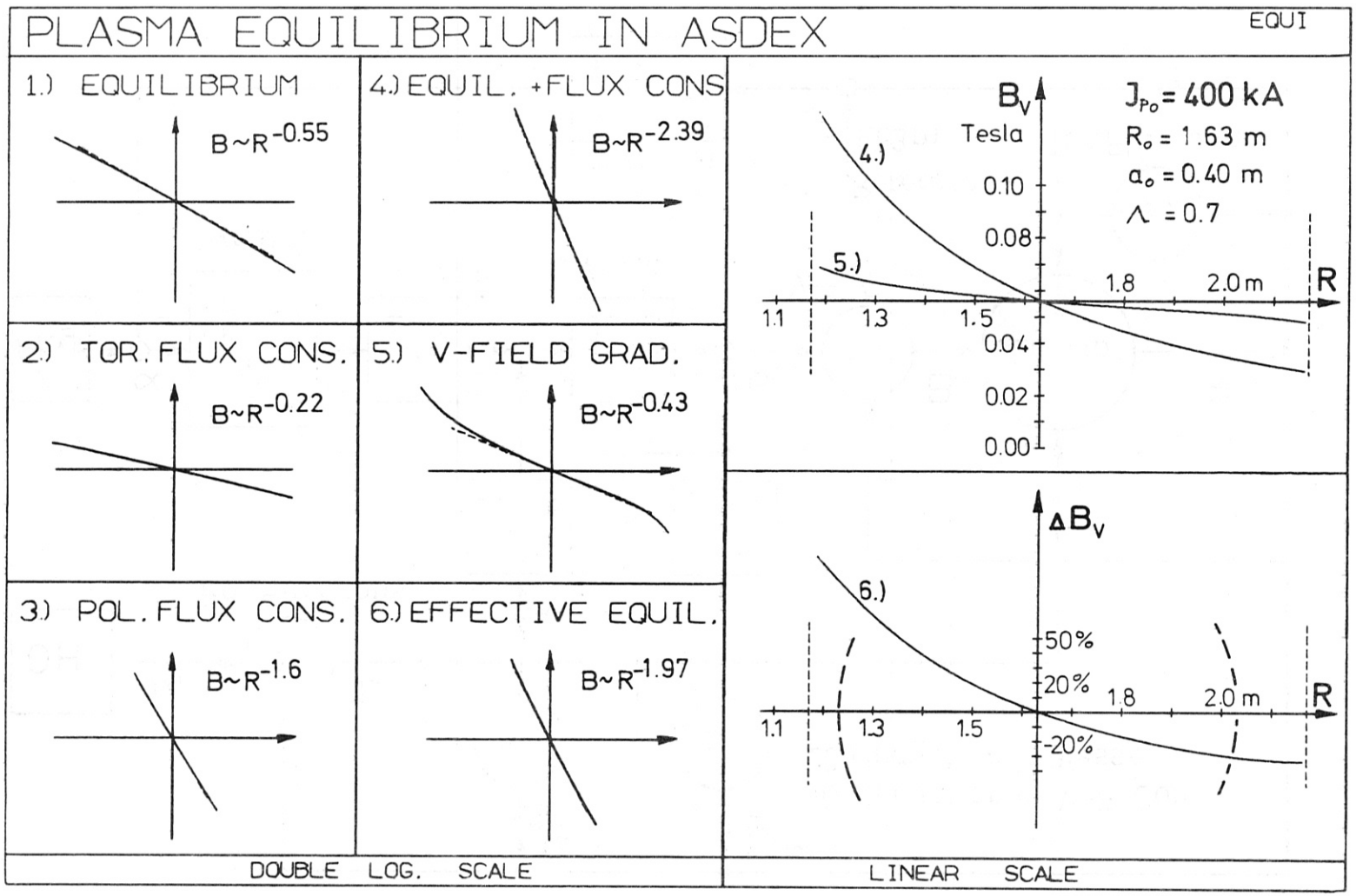
PLASMA EQUILIBRIUM IN ASDEX
EQUI
1.) EQUILIBRIUM
B~R^-0.55
2.) TOR. FLUX CONS.
B~R^-0.22
3.) POL. FLUX CONS.
B~R^-1.6
4.) EQUIL. + FLUX CONS
B~R^-2.39
5.) V-FIELD GRAD.
B~R^-0.43
6.) EFFECTIVE EQUIL.
B~R^-1.97
DOUBLE LOG. SCALE
B_V
Tesla
J_Po = 400 kA
R_o = 1.63 m
a_o = 0.40 m
Λ = 0.7
4.)
5.)
0.10
0.08
0.04
0.02
0.00
1.1
1.3
1.5
1.8
2.0 m
R
ΔB_V
6.)
50%
20%
-20%
LINEAR SCALE

Fig.2 /

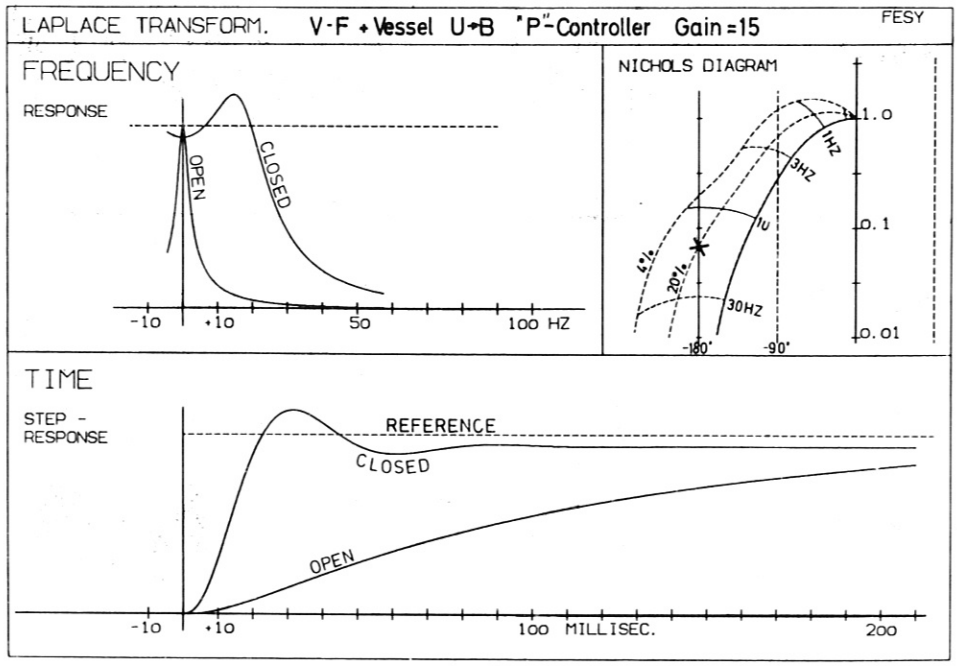

Fig.3

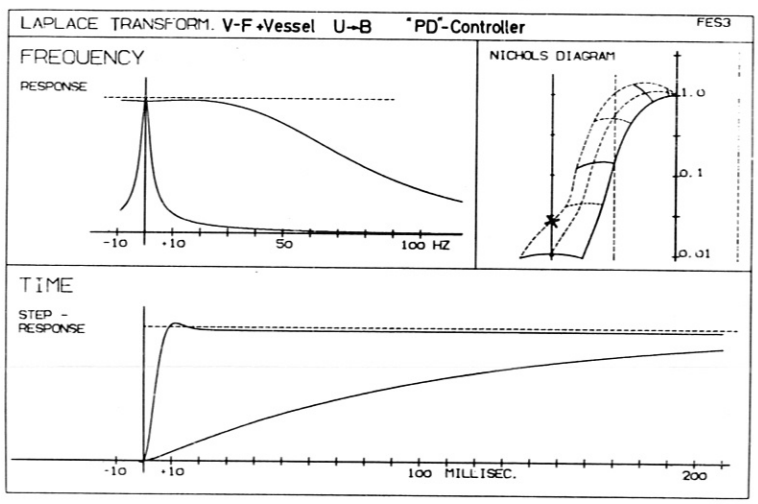

Fig.4

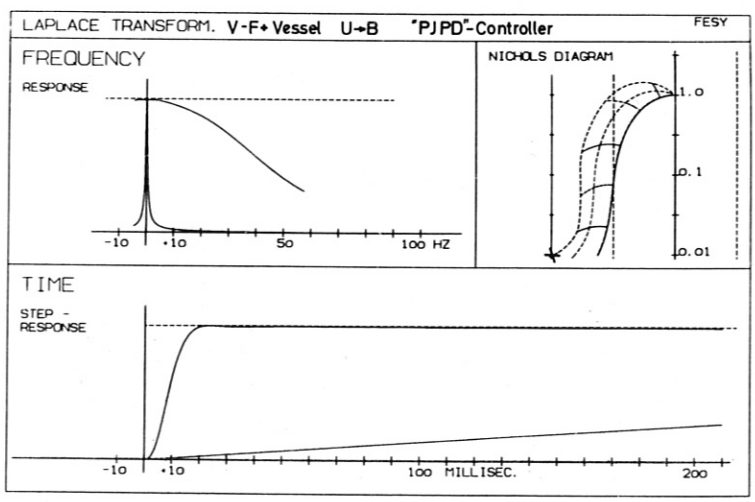

Fig.5

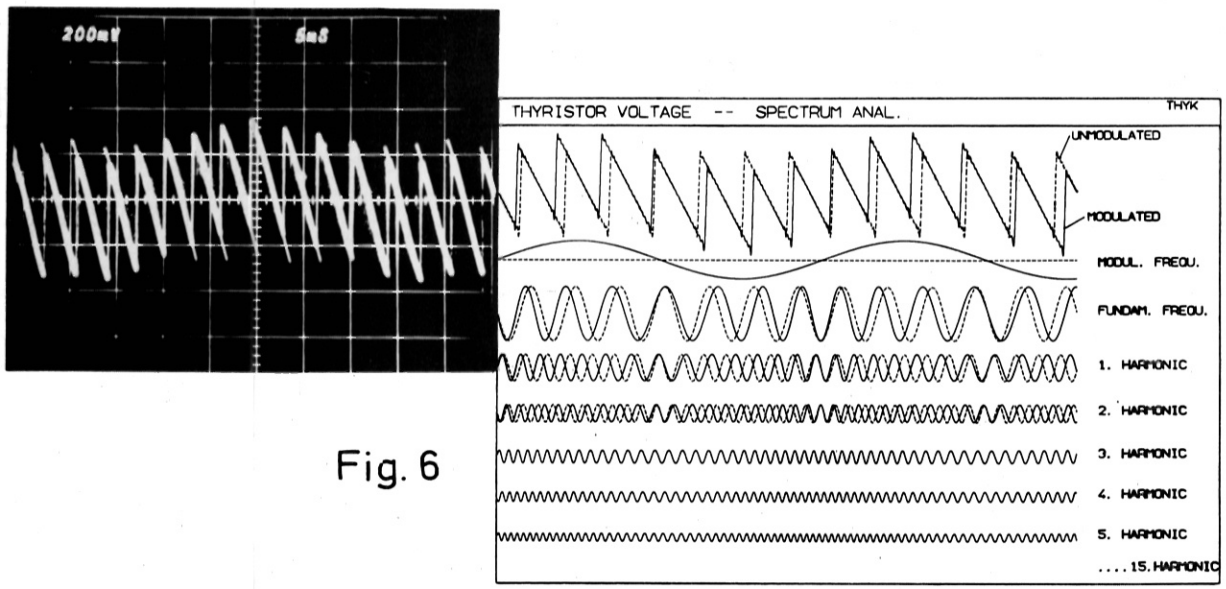

Fig. 6

Thyristor Spectrum

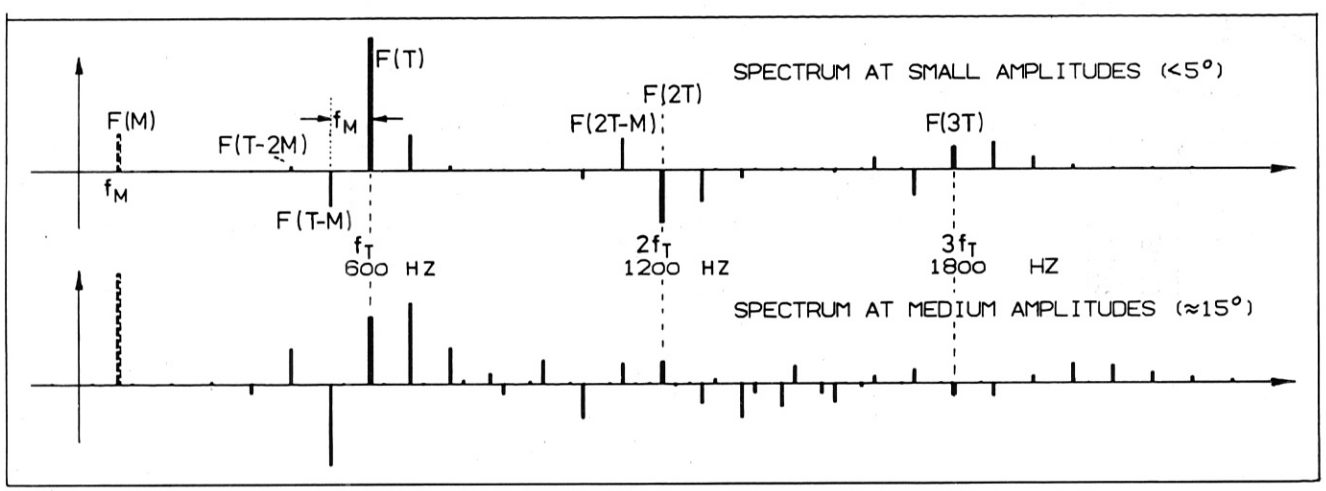

Fig. 7

Fig.8

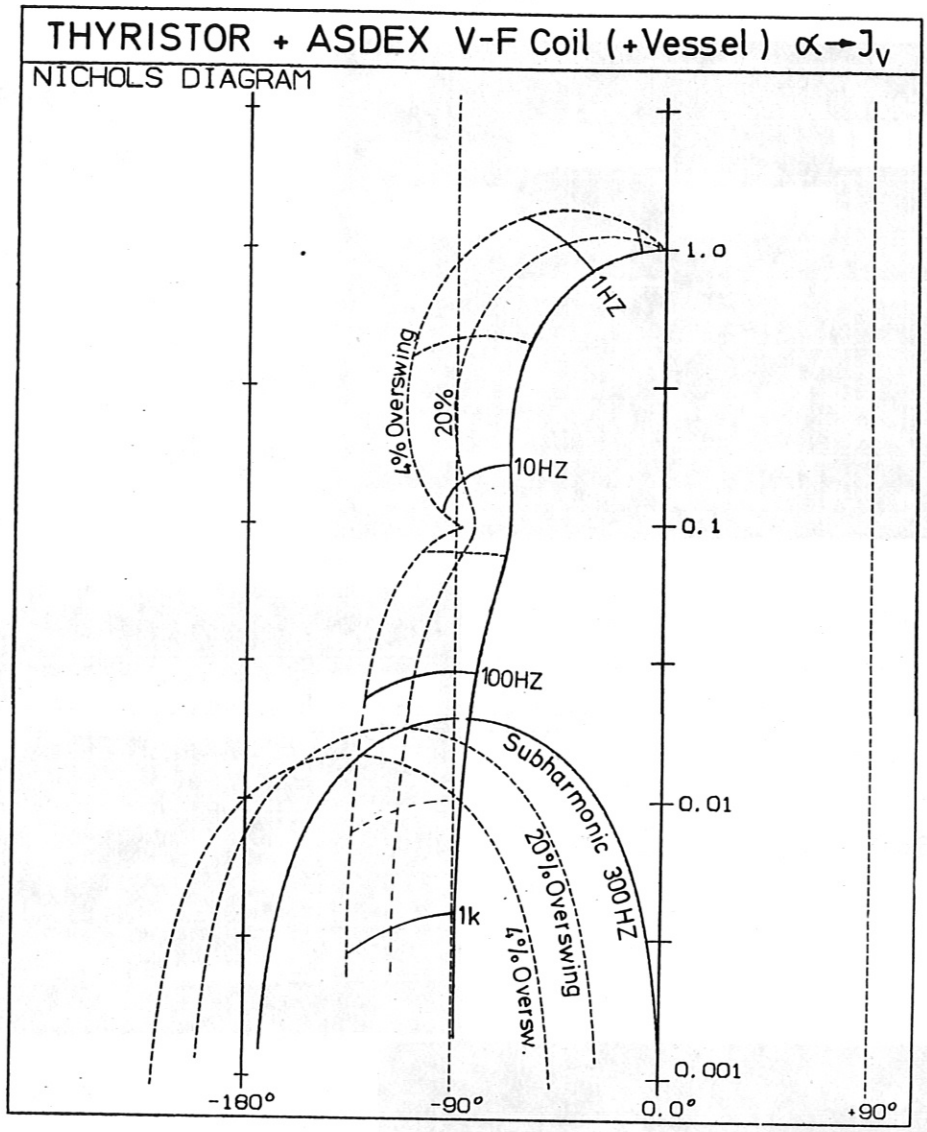

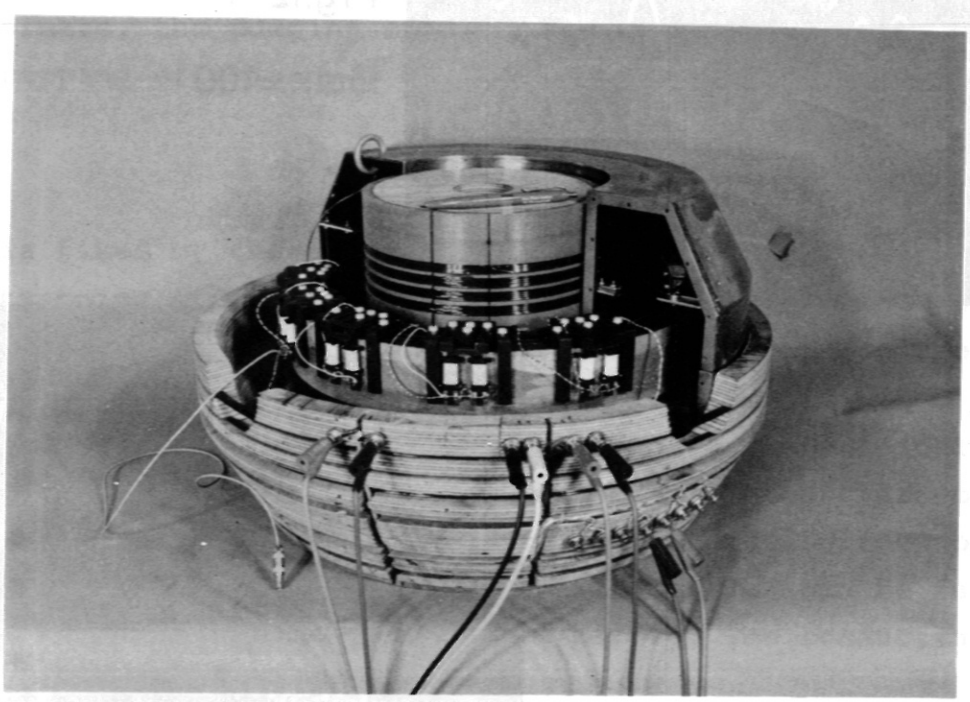

Fig.9 View of the ASDEX Model 1:10

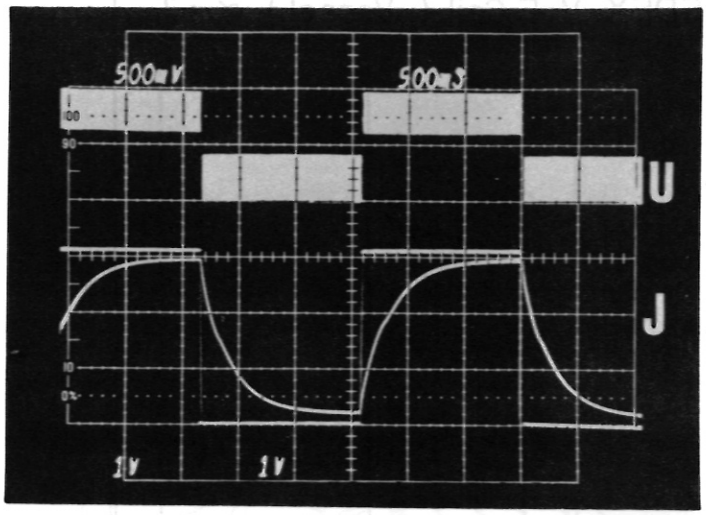

Thyristor +
ASDEX V-F Coil
+(Vessel)

$\propto \rightarrow J_V$

Fig.10
Open loop

Fig.11

Closed loop Gain =10

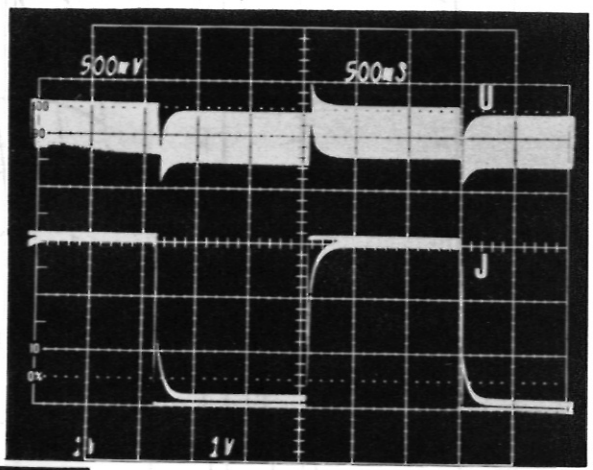

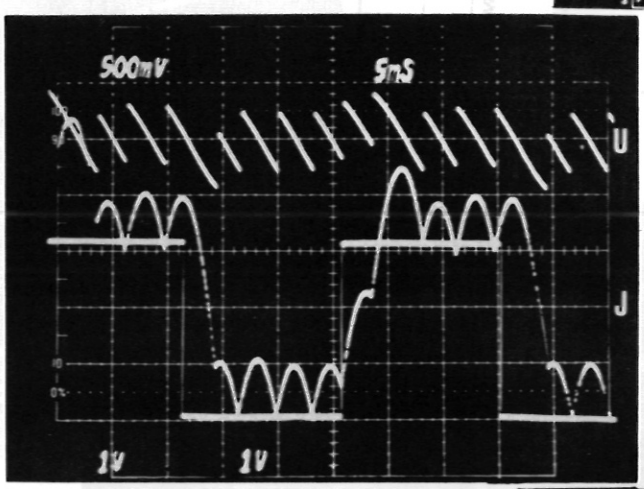

Fig.12

Gain =100

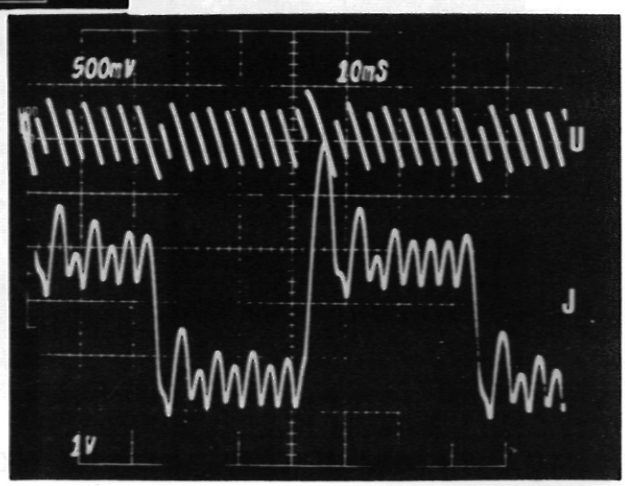

Fig.13

Gain =130

DIVERTOR PUMPING SYSTEM OF ASDEX

G.Haas, M.Keilhacker, W.Poschenrieder, F.Wagner

Abstract

For the divertor pumps in ASDEX speeds for H_2 of several 10^6 l/sec are required. Initially two alternativ concepts were persued: Volume getter pumps based on ST101 and Ti sublimation pumps with cryogenic surfaces. Though both concepts turned out to be feasible, preference was finally given to Ti sublimation pumping, because its efficiency is less dependent on the plasma conditions in the divertor. For this reason the following paper renders a more detailed description for the Ti sublimation pumps only.

1. Introduction

One important characteristic of a divertor is the back-streaming ratio, i.e. the fraction of incoming plasma which returns as neutral gas to the discharge chamber. The back-streaming ratio f_D depends on the conductance C of the divertor throats, the pumping speed S of the divertor pumps and the trapping efficiency σ of the collector rails:

$$f_D = \frac{C}{C + S} (1 - \sigma)$$

As C is fixed by the design of the experiment and a reasonable trapping efficiency in the collector rails cannot readily be achieved, f_D is primarily governed by the pumping speed S.

The ASDEX divertor experiment /1/ will have two poloidal divertors one in the upper and one in the bottom third of the vaccum vessel. They are divided in toroidal direction into 2 x 16 divertor chambers, of which only 26 can be fully used for pumping purposes, and two partly. The conductance of

the divertor throats will be approximately 6×10^5 l/sec. We are aiming at a backstreaming ratio of $f_D < 0.1$.

Two concepts for the divertor pumping system have been investigated:

1. Volume getter pumps
2. Ti sublimation pumps

2. Volume Getter Pumps

This pumping system would utilize commercial-type getter cartridges (SAES, SORBAC C500 m), cylindrical structures of folded thin constantan sheets coated with a Zr/Al alloy which pumps H_2 reversibly. The specific design was developed by SAES under a study contract No.52658/DT in which essential performance characteristics such as anticipated for ASDEX conditions were also investigated. The studies included Monte Carlo calculations of the backstreaming ratio and problems such as the sensitivity to contamination of the working gas H_2 with O_2, N_2 or CO. The investigation showed the basic feasibility of this system, but, owing to the spatial limitation in ASDEX, the attainable pumping speed could not exceed 2×10^6 l/sec. Accordingly, the backstreaming ratio would be well above 0.2 if not backed by additional gas trapping in the collector rails. Theoretical work /2/ shows that under favorable conditions $\sigma > 0.6$ may be expected, which here would indeed result in $f_D < 0.1$. Measurements below 1.5 keV /3/, however, showed a pronounced decrease in the trapping efficiency not explained by theory which indicates some contamination problems. In ASDEX we have to take into account a mean proton energy at the collector rails well below 1.5 keV. At present a large parameter range in the backstreaming ratio is considered most important for the evaluation of optimum working conditions. In this respect, the uncertainties associated with this pumping concept caused us to decide in favor of Ti sublimation.

3. Ti Sublimation Pumps

Without trapping in the collector rails it is necessary to have a pumping speed of 6×10^6 l/sec. Estimations and measurements made on a test chamber showed that this pumping speed can be attained by using a Ti sublimation pump system with cryogenic surfaces.

The planned pump system is to have two directly heated sublimators in each divertor chamber. In 26 chambers there are coolable getter panels and in two chambers deposition occurs directly on the vessel surface. A total geometrical area of 90 m^2 is coated, approx. 55 m^2 of this being panels and the remainder uncovered parts of the vacuum vessel or other components. The remainder stays roughly at room temperature. The panels can be cooled with LN_2 or GN_2, their temperature being about 80 - 100 K or 270 - 370 K, respectively. They are made of extruded Al profiles and have to be assembled from laminae which are welded at one end to the coolant pipe and, for the rest, are insulated from one another in order to reduce the forces in the event of a plasma disruption. The laminae profile is designed so as to give a serrated surface on the inside of the panels to enlarge the pump surface. Fig. 1 shows a cross-sectional view of the divertor chamber with the position of Ti sublimators and getter panel.

The cooling- and heating system for the panels is shown schematically in Fig.2. For the stationary cooling at LN_2-temperature (80 - 100 K) a closed cycle is formed from the panels DIV, the pressure tank D_2, the coolant pump C_1 and the heat exchanger E_1. The LN_2 contained in the cycle is subjected to a pressure of 11 bar to avoid local boiling. For all other modes of operation including baking the panels are charged with GN_2 in an open cycle. The temperature of the GN_2 can be set with the three-way valve V, the heat exchanger

E_3 and the electrical heater E_2. The design of the panels and the cooling and heating system is developed by LINDE under a study contract (Komm.No.5484/0290).

The main problems incurred with such a pump system are

- capacity of a Ti layer
- Ti supply in the sublimators
- adhesion of the deposited Ti layers

These questions are being investigated in a test chamber, representing a 1 : 1 model of a divertor chamber. A geometrical area of 3.5 m^2 can be coated with Ti, 1 m^2 of it being an Al panel that can be cooled with LN_2 or compressed air. The test cycle, which is fitted to the pulsed operation planned for ASDEX, consists of Ti sublimation for 30 - 90 sec, a waiting period of 30 - 90 sec, a gas pulse of 0.15 - 0.35 torr l H_2 and a further waiting period of 200 sec. The gas inflow attains its maximum in 80 msec and is completed after 500 msec. The pumping speed and capacity can only be regarded as lower limits for ASDEX. Whereas only molecular H_2 occurs in the test chamber, a part of the hydrogen in the divertor is atomic. Molecular hydrogen, however, has a lower sticking probability than atomic hydrogen. According to a model of Simonov et al. /4/ it is bound to cryogenic Ti surfaces without dissociation so that it cannot diffuse inwards.

Atomic hydrogen affords the following advantages /5/:
The pumping speed is higher at least on warm surfaces. As result, the cold surfaces have to cope with less hydrogen and do not saturate so fast. It appears that atomic hydrogen can also diffuse into cold Ti surfaces so that more than one monolayer is bound. As the atomic component of the gas in the divertor is not yet known, no quantitative information can be obtained.

Capacity

The capacity is the quantity of gas that can be pumped in a short time without the pumping speed dropping below the permissible value. It has to be compatible with the quantity of gas occurring during a discharge. For a discharge time of 10 confinement times after the current rise time and a mean proton density of $2 - 5 \times 10^{13} cm^{-3}$ this quantity is 25 - 45 torr l hydrogen. While the pumping speed is high enough at the start even for pure molecular hydrogen, this does not apply to the capacity. Scaling our test results to ASDEX, we attain with fresh Ti layer a pumping speed of 17×10^6 l/sec, which, however, drops below 5×10^6 l/sec after gettering of 12 torr l molecular hydrogen. With the effects of the atomic component the divertor capacity should be sufficient for low-density discharges. This is probably no longer true at high densities. For such discharges it is intended to use warm panels. The pumping speed is then lower from the start, but tends to remain constant. Figure 3 shows the time behavior of the pumping speed which we attain in our test chamber with cooled and with uncooled panel. For high density discharges a higher backstreaming ratio seems acceptable, as the plasma contamination should be lower even without divertor action.

Ti Supply

The design of the Ti sublimators must meet three requirements. The Ti supply should be sufficient for 2,000 - 3,000 discharges, the sublimators should be mounted from the outside, and they should represent line sources 0.5 - 1 m in length since their distance from the panels is much less than the dimensions of the panels. As approx. 0.4 g Ti has to be evaporated to getter 25 torr l H_2 the supply of Ti that can be evaporated has to be 1200 g. Because of the third requirement, point sources such as electron beam sublimators or the Ti-ball of Varian are out of question. All requirements can be

met by connecting directly heated commercial Ti/Mo wires in parallel. Our sublimators (Fig.4) consist of an uncooled high current feed-through for 800 - 1000 A on a 4 1/2" CF flange and two parallel Cu bars between which the Ti/Mo wires are clamped. We have operated such sublimators under various pulsed conditions evaporating 0.3 - 1.5 mg Ti per puls and wire until 40 - 70 % of the wires in a sublimator burned out. In all cases we could evaporate an average of 1.1 g Ti from wires with an initial weight of 3.7 g. It thus follows that the sublimators have to be provided with approx. 20 wires. Resistance variations of up to 20 % between the parallel wires e.g. by a winding short in coiled wires were found to be of no consequences. A wire of lower resistance draws more current, becomes hotter and evaporates faster until its resistance is equalized to that of the other wires.

Peeling

Peeling of the deposited Ti layers can never be completely avoided. For ASDEX this means that the panels have to be cleaned at regular intervals, and so they are designed for easy dismounting. To make the intervals as long as possible, it has hitherto been found best to make the surface as rough as possible besides ensuring thorough cleaning.

Conclusions

Considering the principal aims of the experiment ASDEX, Ti sublimation on cryogenic surfaces appeared here to be the better choice for divertor pumping, as there is no problem to achieve a low backstreaming ratio and it is an approved pumping concept. It is quite obvious to us, however, that in divertor machines closer to a CTR, Ti sublimation will no longer be practicable because of the high temperature environment and the need for a safe tritium handling system. Under these conditions volume getters which reversibly pump hydrogen should be more appropriate.

References

/1/ R.Allgeyer et al., Proc.6th Symp.on Engineering Problems in Fusion Research, San Diego 1975, p.378

/2/ M.T.Robinson, Proc.3rd Conf.on Atomic Collissions with Solids, Kiew 1974

/3/ J.Bodansky, J.Roth, W.Poschenrieder, Inst.Phys.Conf. Ser.No.28, (1976) p.307
M.K.Sinha, J.Roth, J.Bodansky, Proceedings of 9th Symp. on Fusion Technology, Garmisch 1976, paper A 1-4

/4/ V.A.Simonov et al., Nucl.Fusion suppl.1 (1962) 325

/5/ G.D.Martin, Report MATT 1193 (1976)

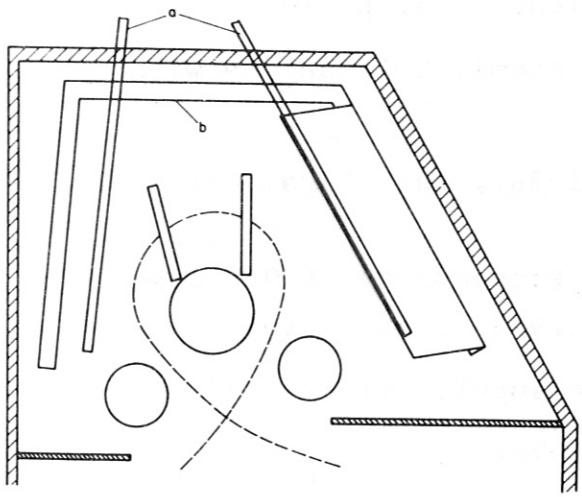

Fig.1: Cross-section of ASDEX-divertor chamber schowing the location of the Ti-sublimators (a) and the geeter panel (b).

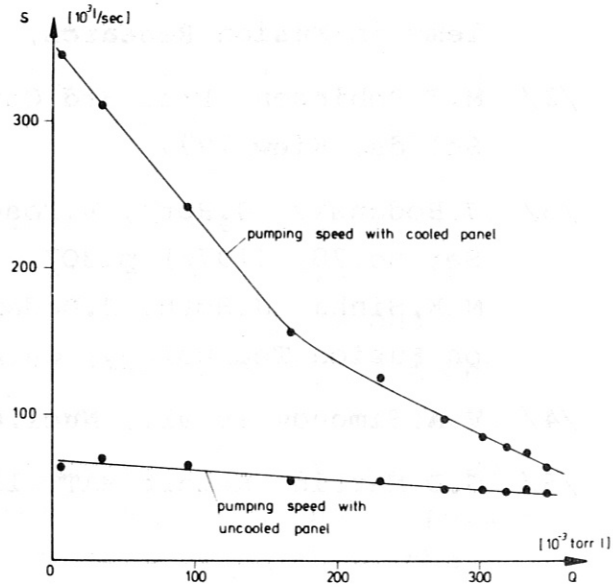

Fig.3: Pumping speed versus sorbed H_2-quantity with getter panels cooled and uncooled

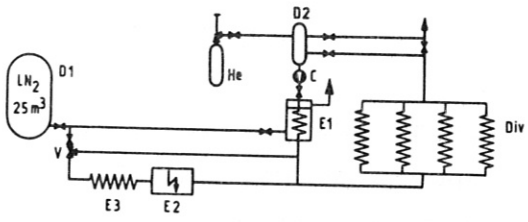

Fig.2: Schematic of the cooling- and heating system.
Div: Divertor getter panel
C : Coolant pump
E_1, E_3: Heat exchanger
E_2 : Electrical heater
V : Three-way-valve

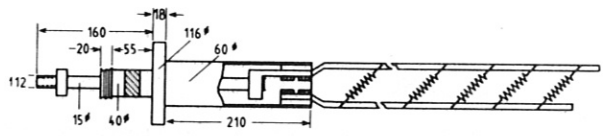

Fig.4: Design of the Ti-sublimator